The characterisation and origin of graphite in cratonic lithospheric mantle: a petrological carbon isotope and Raman spectroscopic study

Article *in* Contributions to Mineralogy and Petrology · February 1994

DOI: 10.1007/BF00320978

CITATIONS
104

READS
168

7 authors, including:

Graham Pearson
University of Alberta
543 PUBLICATIONS **16,237** CITATIONS

SEE PROFILE

Stephen Haggerty
Florida International University
192 PUBLICATIONS **6,409** CITATIONS

SEE PROFILE

Jill Dill Pasteris
Washington University in St. Louis
133 PUBLICATIONS **5,885** CITATIONS

SEE PROFILE

Contrib Mineral Petrol (1994) 115:449–466

Contributions to Mineralogy and Petrology

The characterisation and origin of graphite in cratonic lithospheric mantle: a petrological carbon isotope and Raman spectroscopic study

D.G. Pearson [1]*, F.R. Boyd [2], S.E. Haggerty [3], J.D. Pasteris [4], S.W. Field [5], P.H. Nixon [6], and N.P. Pokhilenko [7]

[1] Department of Terrestrial Magnetism, Carnegie Institution of Washington, 5241 Broad Branch Rd, N.W. Washington, DC 20015, USA
[2] Geophysical Laboratory, Carnegie Institution of Washington, 5251 Broad Branch Rd, N.W. Washington, DC 20015, USA
[3] Department of Geology, University of Massachusetts, Amherst, MA 01003, USA
[4] Department of Earth and Planetary Sciences, Washington University, St. Louis, MO 63130, USA
[5] Department of Geology, Stockton State College, Pomona, NJ 08240, USA
[6] Department of Earth Sciences, University of Leeds, Leeds LS29JT, UK
[7] Institute of Mineralogy and Petrography, Russian Academy of Sciences, Siberian Branch, Novosibirsk, Russia

Abstract. Graphite-bearing peridotites, pyroxenites and eclogite xenoliths from the Kaapvaal craton of southern Africa and the Siberian craton, Russia, have been studied with the aim of: 1) better characterising the abundance and distribution of elemental carbon in the shallow continental lithospheric mantle; (2) determining the isotopic composition of the graphite; (3) testing for significant metastability of graphite in mantle rocks using mineral thermobarometry. Graphite crystals in peridotie, pyroxenite and eclogite xenoliths have X-ray diffraction patterns and Raman spectra characteristic of highly crystalline graphite of high-temperature origin and are interpreted to have crystallised within the mantle. Thermobarometry on the graphite-peridotite assemblages using a variety of element partitions and formulations yield estimated equilibration conditions that plot at lower temperatures and pressures than diamondiferous assemblages. Moreover, estimated pressures and temperatures for the graphite-peridotites fall almost exclusively within the experimentally determined graphite stability field and thus we find no evidence for substantial graphite metastability. The carbon isotopic composition of graphite in peridotites from this and other studies varies from $\delta^{13}C_{PDB} = -12.3$ to -3.8‰ with a mean of -6.7‰, $\sigma = 2.1$ ($n = 22$) and a mode between -7 and -6‰. This mean is within one standard deviation of the -4‰ mean displayed by diamonds from peridotite xenoliths, and is identical to that of diamonds containing peridotite-suite inclusions. The carbon isotope range of graphite and diamonds in peridotites is more restricted than that observed for either phase in eclogites or pyroxenites. The isotopic range displayed by peridotite-suite graphite and diamond encompasses the carbon isotope range observed in mid-ocean-ridge-basalt (MORB) glasses and ocean-island basalts (OIB). Similarity between the isotopic compositions of carbon associated with cratonic peridotites and the carbon (as CO_2) in oceanic magmas (MORB/OIB) indicates that the source of the fluids that deposited carbon, as graphite or diamond, in cratonic peridotites lies within the convecting mantle, below the lithosphere. Textural observations provide evidence that some of graphite in cratonic peridotites is of sub-solidus metasomatic origin, probably deposited from a cooling C–H–O fluid phase permeating the lithosphere along fractures. Macrocrystalline graphite of primary appearance has not been found in mantle xenoliths from kimberlitic or basaltic rocks erupted away from cratonic areas. Hence, graphite in mantle-derived xenoliths appears to be restricted to Archaean cratons and occurs exclusively in low-temperature, coarse peridotites thought to be characteristic of the lithospheric mantle. The tectonic association of graphite within the mantle is very similar to that of diamond. It is unlikely that this restricted occurrence is due solely to unique conditions of oxygen fugacity in the cratonic lithospheric mantle because some peridotite xenoliths from off-craton localities are as reduced as those from within cratons. Radiogenic isotope systematics of peridotite-suite diamond inclusions suggest that diamond crystallisation was not directly related to the melting events that formed lithospheric peridotites. However, some diamond (and graphite?) crystallisation in southern Africa occurred within the time span associated with the stabilisation of the lithospheric mantle (Pearson et al. 1993). The nature of the process causing localisation of carbon in cratonic mantle roots is not yet clearly understood.

*Now at: Department of Earth Sciences, The Open University, Walton Hall, Milton Keynes MK7 6AA, UK

Correspondence to: D.G. Pearson

Introduction

Carbon or carbon-bearing species in the mantle have received much attention due to their possible role in magma genesis (Bailey 1980; Eggler and Baker 1982; Spera 1984; Taylor and Green 1989). Carbon may also

influence mantle f_{O_2} (e.g. Wood 1991) and physical properties (Duba and Shankland 1982) and plays an intrinsic role in diamond formation (e.g. Boyd and Gurney 1986; Gurney 1991). Hence, knowledge of the distribution and origin of carbon and carbonaceous phases in the mantle is important in constraining its role in several mantle processes. One form of mantle carbon that has received little attention is macrocrystalline graphite. Peridotite xenoliths bearing discrete macrocrystalline grains of graphite are as rare as diamondiferous peridotites yet, despite their importance in the study of mantle volatiles, they have received only passing attention in the literature (Wagner 1916; Mathias et al. 1970; Nixon and Boyd 1973a, Boyd and Nixon 1975; Sobolev 1974; Rodionov and Sobolev 1985; Nixon et al. 1987; Field and Haggerty 1990; Pearson et al. 1990; Schulze and Valley 1991).

Most oxidised forms of carbon such as kimberlite carbonates, CO_2 inclusions in mid-ocean-ridge basalts (MORB) and ocean-island basalts (OIB) and also some reduced carbon such as the coats of coated diamonds, are believed to have grown directly from CO_2-H_2O rich fluids derived from the convecting mantle. Their carbon isotopic compositions lie within a limited range ($\delta^{13}C \sim -4$ to -10‰) similar to that of MORB/OIB (Deines and Gold 1973; Javoy et al. 1986; Nadeau et al. 1990; S.R. Boyd et al. 1992). The origin of reduced, elemental carbon, predominantly from the subcontinental lithosphere, is more controversial. Diamonds show a large range in carbon isotopic composition ($\delta^{13}C \sim -34$ to $+4$‰), the range for diamonds of peridotite paragenesis (P-type) being much more restricted than those of eclogite suite paragenesis (E-type; Sobolev et al. 1979; Galimov 1991). There is no general consensus as to the origin of the large isotopic range in diamonds or the difference between E- and P-type populations. Current models include fractionation from a parental reservoir similar to MORB/OIB (Javoy et al. 1986), formation from an isotopically heterogeneous mantle (Deines 1991) and formation of E-type diamonds from subducted crustal material (Sobolev and Sobolev 1980; Milledge et al. 1983; Gurney 1991). Most work on reduced carbon in the mantle has been carried out on diamonds; there are few reported analyses of graphite (Kropotova and Fedorenko 1970; Pearson et al. 1990; Schulze and Valley 1991). Study of graphite in mantle rocks allows direct comparison between two distinct forms of reduced mantle carbon, diamond and graphite, originating at different depths. These data can be used to test the suggestion that there is vertical C isotopic stratification in the mantle (Deines et al. 1991) and to further examine the distinction between carbon associated with peridotite and eclogite lithologies.

The influence of reduced carbon on mantle melting relations and its large oxygen buffering capacity makes it important to know the nature and distribution of such phases in the mantle. Furthermore, knowledge of the origin of diamond and graphite would provide constraints on the volatile outgassing and recycling budget of the Earth. In addition, graphite and diamond in mantle xenoliths can be used to constrain their depth of origin (e.g. Finnerty and Boyd 1984, 1987), and hence reveal the thermal structure beneath cratons (McKenzie 1989), if it can be shown that they have crystallised stably. Experimentally and empirically formulated geobarometers can be tested by observing whether $P-T$ estimates for diamond- or graphite-bearing peridotites are consistent with the diamond-graphite transition (Finnerty and Boyd 1984, 1987). This approach has previously suffered from the scarcity of data for graphite-bearing peridotites. Moreover, it is necessary to show that the graphite equilibrated with the host silicate assemblages at depth in the mantle and did not form by secondary processes within the crust.

This study aims to address the above problems by detailed petrological study, X-ray and Raman characterisation of graphite, mineral thermobarometry and carbon isotope analyses of graphite in peridotite, eclogite and pyroxenite xenoliths from kimberlites. Graphite-bearing samples were obtained from large xenolith collections at the University of Leeds, the University of Massachusetts and the Geophysical Laboratory with supplementary material from the Institute of Mineralogy and Petrology, Novosibirsk. An extensive collection of xenoliths from the Premier kimberlite and the Kimberley Pipes, R.S.A., were also examined in order to estimate the frequency of occurrence of graphite in the lithospheric mantle.

Occurrence

Graphite is described from 26 xenoliths from various kimberlite localities; 24 samples are from southern Africa and 2 are from Siberia. Of these, 19 are lherzolites or harzburgites, 3 are pyroxenites, 2 are megacrysts and 2 are eclogites (Appendix 2). All the peridotites are of the coarse, low-temperature variety, believed to be derived from the lithospheric mantle (Nixon and Boyd 1973b). The graphite-bearing xenoliths were collected from kimberlites erupted along the southern margin of the Kaapvaal craton (Kimberley, Jagersfontein and northern Lesotho), the Premier pipe in the central part of the Kaapvaal craton and from the Udachnaya and Obnazhennaya kimberlites in the Siberian craton. There appear to be no recorded occurrences of mantle-derived xenoliths containing macrocrystalline graphite of primary appearance in either kimberlites or alkali basalts erupted in circum-cratonic areas. No mantle graphite has been recorded in extensive kimberlite xenolith collections from off-craton areas in southern Africa, including East-Griqualand, the Karoo and Namibia. Moreover, we know of no description of primary appearing graphite in peridoties from basaltic volcanoes in western North America (H. Wilshire and A.J. Irving personal communication, 1991), Europe, southeastern Australia, or elsewhere. Additionally, graphite has not been found in any high-temperature (sheared) peridotites, although in off-craton areas some of these high-temperature peridotites appear to have originated within the graphite stability field (Finnerty and Boyd 1987). The only known occurrences of macrocrystalline, highly ordered graphite in rocks of undisputed mantle derivation other than xenoliths from cratonic lithosphere are graphitised diamonds in pyroxenites from the Beni Bousera and Ronda orogenic peridotite massifs (Pearson et al. 1989; Pearson et al. 1991a; Davies et al. in press). In these occurrences the graphite is restricted to the pyroxenites.

Girod (1967) and Kornprobst et al. (1987) reported macrocrystalline graphite of apparently primary origin in ultramafic xenoliths from an alkali basalt in the Tissemt area, Hoggar, Algeria. Petrological and geochemical data from the Hoggar samples, however,

indicate that they were probably entrained from a deep crustal layered intrusion and are thus not of direct mantle origin (Kornprobst et al. 1987). The apparent restriction of graphite to the subcontinental lithospheric mantle keels underlying Archaean cratons is similar to the strong association of diamonds with Archaean cratons (Kennedy 1964; Boyd and Gurney 1986).

Mineralogy and Petrography

Xenoliths

Graphite-bearing peridotites addressed in this study include garnet harzburgites that exhibit variable depletion in Ca, garnet-spinel lherzolites, garnet lherzolites, a spinel-facies peridotite and three pargasite (amphibole) peridotites. Three of the graphite-bearing harzburgites and some from the suite studied by Viljoen et al. (in press) contain subcalcic high-chrome pyrope garnets; however, many fall within the Ca-saturated garnet field indicative of lherzolitic paragenesis (Sobolev 1974), Table 1, Fig. 1. The wide variety of garnet compositions and xenolith lithology suggests that there is no specific lithological association for graphite occurrences. Diamondiferous southern African peridotite *xenoliths* contain both Ca-saturated and undersaturated garnet (Dawson and Smith 1975; Shee et al. 1982; Viljoen et ala. 1992), also indicating no specific lithological bias of diamonds *in xenoliths* (Fig. 1). Peridotite suite garnets included in diamonds from southern Africa show a large compositional range, encompassing the range for garnets from graphite- and diamond-bearing peridotite *xenoliths* (Fig. 1). However, although there is much compositional variation, the majority of *diamonds* of peridotite affinity from both southern Africa and Siberia contain garnets that are undersaturated in Ca and high in Cr (knorringite component ; Sobolev et al. 1984; Boyd and Gurney 1986; Boyd et al. 1993).

The scarcity of previously documented graphite-bearing peridotite xenoliths may in part be due lack of purposeful screening. A meticulous search of over 200 peridotite xenoliths from the Premier mine, South Africa, yielded 5 graphite-bearing specimens, i.e. around 2.5% of the total population. A comparable search of 63 peridotites from the Bultfontein floors, Kimberley, yielded only one containing graphite. Seven graphite-bearing xenoliths (6 peridotites and an eclogite) have been found by us at Jagersfontein from approximately 800 samples (<1%). However, a greater frequency must be present in some portions of the kimberlite at Jagersfontein because 20 graphite-bearing eclogites were described by Wagner (1916) in the early days of mining. The recorded frequency of graphite at Premier is higher than that recorded for diamondiferous specimens at most localities, but it should be noted that diamond has been found in over 2% of all megacrystalline peridotites at Udachnaya, Siberia.

Of special interest is an exsolved megacrystic specimen from southern Africa, which is possibly derived from low-temperature pyroxenites. Samples of this type do not appear to be part of the chrome-poor, discrete megacryst suite evident in some kimberlites (Nixon and Boyd 1973c). Two pyroxenite xenoliths from Premier are olivine websterites/orthopyroxenites. One from Obnazhennaya is a high-temperature orthopyroxenite, which has cooled to exsolve abundant blebs and lamellae of garnet and chrome diopside from the enstatite. Graphite has been reported previously in orthopyroxene-rich websterites from Siberian kimberlites by Galimov et al. (1989). Although much of the graphite in the xenoliths described by Galimov is intergrown with phlogopite, we see no relationship to phlogopite in any of the pyroxenites studied here. Graphite was also found in an ilmenite-rutile-bearing eclogite (PHN 2793/8B Appendix 2). The garnet composition in this rock (high Fe, low Ca) is indicative of a crustal origin (Table 1).

Graphite morphology

In the samples studied here, graphite most commonly occurs as dispersed, subhedral to euhedral flakes and multicrystalline stacks

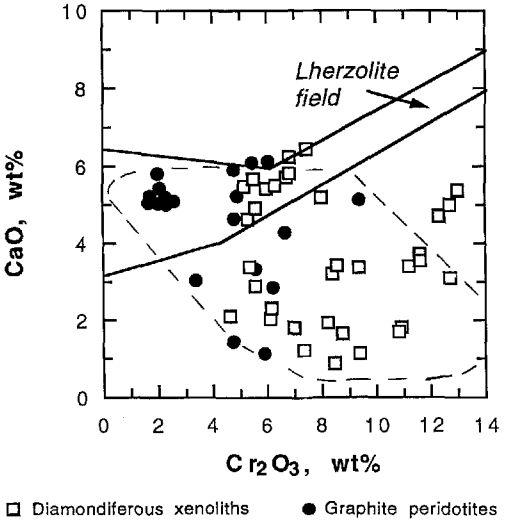

Fig. 1. CaO and Cr_2O_3 contents of garnets from graphite- and diamond-bearing peridotite xenoliths. Lherzolite field is from Sobolev (1974). *Dashed line* encloses the field for P-type diamond inclusions. Data from this study, Dawson and Smith (1975), Shee et al. (1982), Sobolev et al. (1984), Radionov and Sobolev (1985), Pokhilenko et al. (1991) and unpublished, Viljoen et al. (1992) and Viljoen et al. (in press)

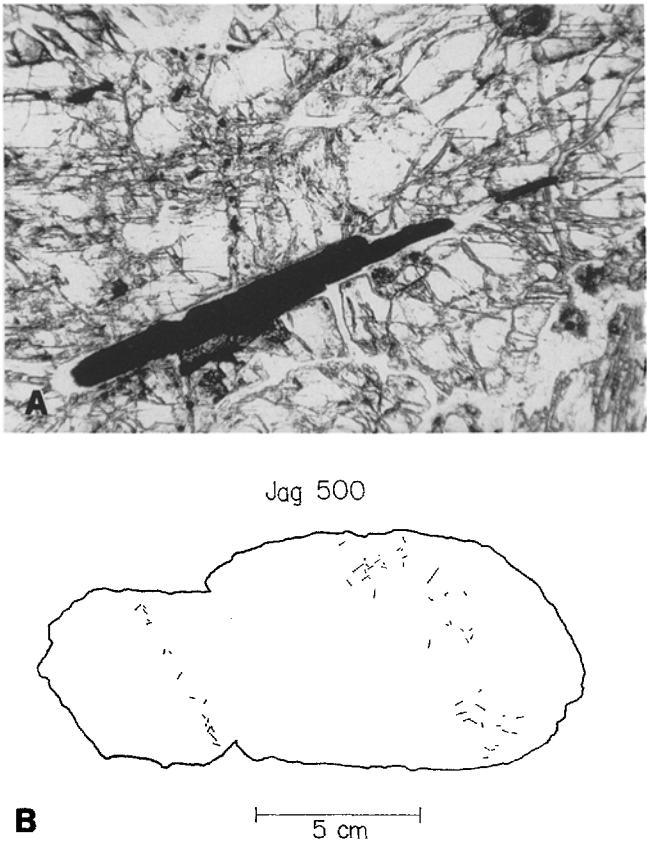

Fig. 2. a Photomicrograph of graphite-bearing pargasite garnet peridotite PHN5633 from Jagersfontein, showing coarse grains of enstatite completely enclosing a lath of graphite. Width of the field of view is 2.35 mm. **b** Line drawing of the distribution of graphite in specimen JAG 84-500 showing vein-like distribution of graphite

Table 1. Mineral compositions of graphite-bearing xenoliths. Elements labeled <0.03 were below the detection limit and those designated, –, were not analysed. Additional data: PHN2826B, Nixon et al. (1987); PHN1569, Boyd and Finger (1975); PHN2265, Nixon and Boyd 1973a

	FRB 888				E-8			
	Olivine	Enstatite	Garnet	Spinel	Olivine	Estatite	Garnet	Spinel
Na_2O	–	<0.03	<0.03	–	–	0.04	<0.03	–
MgO	52.1	37.0	22.3	13.5	52.3	35.8	20.5	14.3
Al_2O_3	<0.03	0.75	20.4	10.4	<0.03	0.79	19.3	10.5
SiO_2	41.4	58.0	42.1	0.12	40.8	57.3	41.8	0.21
K_2O	–	–	–	–	–	–	–	–
CaO	<0.03	0.32	4.63	<0.03	0.03	0.43	6.12	<0.03
TiO_2	<0.03	<0.03	<0.03	0.09	<0.03	<0.03	<0.03	0.03
Cr_2O_3	<0.03	0.36	4.79	59.8	<0.03	0.36	6.04	58.3
MnO	0.08	0.11	0.36	0.32	0.12	0.12	0.33	0.26
FeO	6.69	4.09	6.41	12.8	6.93	3.84	6.13	11.3
Fe_2O_3	–	–	–	2.85	–	–	–	3.59
NiO	0.42	0.11	<0.03	0.13	0.44	<0.03	<0.03	0.04
Total	100.7	100.9	101.1	99.8	100.6	98.6	100.2	98.5

	PHN 2492			PHN 2826B			
	Olivine	Enstatite	Garnet	Olivine	Enstatite	Garnet	Spinel
Na_2O	–	<0.03	<0.03	–	<0.03	<0.03	–
MgO	51.65	37.0	22.6	53.8	37.0	23.68	17.5
Al_2O_3	<0.03	0.66	19.3	<0.03	1.36	21.9	27.9
SiO_2	41.3	58.2	42.5	41.9	57.1	43.0	0.21
K_2O	–	–	–	–	–	–	–
CaO	0.04	0.34	4.27	<0.03	0.15	3.04	<0.03
TiO_2	<0.03	<0.03	<0.03	<0.03	<0.03	<0.03	<0.03
Cr_2O_3	0.03	0.38	6.65	<0.03	0.32	3.38	43.7
MnO	0.10	0.10	0.34	0.03	0.07	0.35	0.24
FeO	6.64	4.05	6.04	5.36	3.52	6.26	9.90
Fe_2O_3	–	–	–	–	–	–	1.16
NiO	0.39	<0.03	<0.03	0.36	<0.03	<0.03	<0.03
Total	100.2	100.8	101.7	101.4	99.5	101.7	100.5

	PHN 5633				PHN 2265		
	Olivine	Enstatite	Garnet	Amphibole	Olivine	Enstatite	Diopside
Na_2O	–	<0.03	<0.03	3.64	<0.03	0.06	<0.03
MgO	51.9	37.3	20.6	20.42	52.3	37.0	17.9
Al_2O_3	<0.03	0.68	22.3	11.7	<0.03	0.61	1.21
SiO_2	41.5	57.5	41.5	45.6	40.9	58.6	55.3
K_2O	–	–	–	0.44	–	–	–
CaO	<0.03	0.18	5.03	11.1	0.03	0.48	21.6
TiO_2	<0.03	<0.03	<0.03	<0.03	<0.03	<0.03	
Cr_2O_3	<0.03	0.18	2.03	2.07	<0.03	0.36	1.56
MnO	0.08	0.09	0.49	0.05	0.09	0.10	0.07
FeO	7.58	4.23	7.87	2.08	7.47	0.44	1.77
Fe_2O_3	–	–	–	–	–	–	–
NiO	0.38	0.07	<0.03	<0.03	0.41	0.11	0.04
Total	101.4	100.3	99.8	97.1	101.3	101.8	101.8

Table 1 (continued)

	PHN 1569				JAG 89-5			
	Olivine	Enstatite	Garnet	Diopside	Olivine	Enstatite	Garnet	Diopside
Na_2O	<0.03	0.04	<0.03	1.38	–	0.03	<0.03	1.49
MgO	51.9	36.5	20.2	17.2	50.8	35.6	19.3	17.06
Al_2O_3	0.03	0.95	19.9	2.12	<0.03	0.8	22.9	1.78
SiO_2	41.0	57.3	42.3	54.8	42.0	58.4	42.7	55.3
K_2O	–	–	–	–	–	–	–	–
CaO	<0.03	0.34	6.09	21.5	<0.03	0.15	5.01	21.7
TiO_2	<0.03	<0.03	<0.03	<0.03	<0.03	<0.03	0.04	<0.03
Cr_2O_3	0.03	0.38	5.45	1.6	<0.03	0.21	2.30	1.32
MnO	0.10	0.11	0.44	0.08	<0.03	<0.03	<0.03	<0.03
FeO	7.08	4.21	6.60	1.57	7.06	4.42	8.00	1.14
Fe_2O_3	–	–	–	–	–	–	–	–
NiO	0.48	<0.03	<0.03	<0.03	<0.03	<0.03	<0.03	<0.03
Total	100.6	100.3	101.0	100.3	99.93	99.61	100.1	99.8

	JAG K7-244				JAG 84-292		
	Olivine	Enstatite	Garnet	Diopside	Olivine	Enstatite	Garnet
Na_2O	–	<0.03	<0.03	0.52	–	<0.03	<0.03
MgO	50.4	35.74	18.6	17.7	52.1	36.6	20.3
Al_2O_3	<0.03	0.95	22.5	1.03	<0.03	0.68	21.7
SiO_2	41.9	57.9	42.3	54.6	41.4	57.5	42.4
K_2O	–	–	–	–	–	–	–
CaO	<0.03	0.11	5.81	24.6	<0.03	0.15	5.09
TiO_2	0.05	<0.03	<0.03	<0.03	<0.03	<0.03	<0.03
Cr_2O_3	0.06	0.24	1.99	0.7	<0.03	0.24	2.60
MnO	0.08	0.14	0.64	0.1	0.08	0.11	0.51
FeO	7.31	4.72	8.74	1.18	6.76	4.16	7.48
Fe_2O_3	–	–	–	–	–	–	–
NiO	0.34	<0.03	<0.03	0.04	0.30	0.14	0.04
Total	100.18	99.81	100.6	100.5	100.7	99.6	100.1

	JAG 500			PHN 1555A			PHN4258		
	Olivine	Enstatite	Garnet	Olivine	Enstatite	Spinel	Olivine	Enstatite	Spinel
Na_2O	–	0.06	<0.03	–	<0.03	–	–	<0.03	–
MgO	52.5	36.7	20.3	53.2	35.5	15.9	51.4	36.8	17.7
Al_2O_3	0.04	0.74	21.9	<0.03	1.05	11.9	<0.03	1.66	28.8
SiO_2	41.1	58.3	41.4	41.2	56.9	0.16	40.7	57.7	0.03
K_2O	–	–	–	–	–	–	–	–	–
CaO	0.03	0.17	5.19	<0.03	0.41	<0.03	<0.03	0.36	<0.03
TiO_2	<0.03	<0.03	<0.03	<0.03	<0.03	0.36	<0.03	<0.03	<0.03
Cr_2O_3	<0.03	0.23	2.29	<0.03	0.37	58.2	<0.03	0.37	40.2
MnO	0.08	0.10	0.57	0.11	0.12	0.27	0.08	0.11	0.20
FeO	7.09	4.52	8.33	6.68	3.96	9.93	6.73	4.32	8.90
Fe_2O_3	–	–	–	–	–	3.60	–	–	2.93
NiO	–	<0.03	<0.03	0.45	<0.03	<0.03	0.40	0.07	0.05
Total	100.8	100.8	100.0	101.6	98.3	100.3	99.3	101.4	98.8

Table 1 (continued)

	K7-232					UV404/86			
	Olivine	Enstatite	Garnet	Hige-Fe diopside	Low-Fe diopside	Olivine	Enstatite	Garnet	Diopside
Na_2O	–	<0.03	<0.03	1.05	1.13	–	0.04	<0.03	1.11
MgO	52.2	37.2	20.4	17.4	18.3	51.9	37.2	20.1	17.4
Al_2O_3	<0.03	0.71	22.6	1.59	2.10	<0.03	0.68	20.0	1.48
SiO_2	41.3	58.3	41.6	55.0	55.1	41.1	57.7	40.7	55.0
K_2O	–	–	–	–	–	–	–	–	–
CaO	<0.03	0.15	5.22	23.6	20.6	<0.03	0.35	5.91	22.4
TiO_2	<0.03	<0.03	<0.03	<0.03	<0.03	<0.03	0.02	0.03	<0.03
Cr_2O_3	<0.03	0.13	1.72	0.77	1.73	<0.03	0.22	4.78	1.28
MnO	0.08	0.11	0.52	0.06	0.06	0.10	0.11	0.43	0.08
FeO	6.71	4.42	8.20	1.09	1.97	7.71	4.64	7.49	1.41
Fe_2O_3	–	–	–	–	–	–	–	–	–
NiO	0.41	0.05	<0.03	0.07	0.06	0.36	0.10	0.01	<0.03
Total	100.7	101.1	100.2	100.6	101.0	101.2	101.1	99.4	100.3

	FRB 930B/2					FRB1350				
	Olivine	Enstatite	Garnet	Diopside	Spinel	Olivine	Enstatite	Garnet	Diopside	Spinel
Na_2O	–	0.03	<0.03	1.1	–	–	0.03	<0.03	1.23	–
MgO	51.7	36.6	20.7	17.5	14.5	51.7	36.5	20.1	17.3	13.4
Al_2O_3	<0.03	1.25	22.5	1.85	19.1	0.04	1.13	22.1	2.04	19.3
SiO_2	40.7	58.1	42.2	54.7	0.29	41.0	58.0	42.0	54.9	0.32
K_2O	–	–	–	–	–	–	–	–	–	–
CaO	0.03	0.32	5.05	23.1	0.05	<0.03	0.27	5.43	22.9	0.04
TiO_2	<0.03	<0.03	<0.03	0.03	0.23	<0.03	<0.03	<0.03	<0.03	0.10
Cr_2O_3	<0.03	0.25	1.67	0.80	49.8	<0.03	0.22	2.07	0.90	49.4
MnO	0.08	0.09	0.43	0.07	0.29	0.11	0.10	0.46	0.07	0.029
FeO	7.46	4.65	7.25	1.49	13.2	8.3	5.2	8.23	1.70	14.8
Fe_2O_3	–	–	–	–	2.96	–	–	–	–	2.78
NiO	0.42	0.09	<0.03	0.03	0.09	0.43	0.1	<0.03	0.04	0.09
Total	100.4	101.4	99.8	100.7	100.6	101.6	101.6	100.4	101.1	100.5

	FRB 1384				PHN5235						
	Olivine	Enstatite	Diopside	Spinel	Olivine	High-Al enstatite	Low-Al enstatite	Garnet	Diopside	High-Al spinel	Low-Al spinel
Na_2O	<0.03	0.05	1.15	<0.03	<0.03	0.16	<0.03	<0.03	0.68	–	–
MgO	51.8	34.7	16.4	17.1	51.7	36.4	36.8	20.1	17.9	15.9	14.4
Al_2O_3	<0.03	3.3	3.97	37.1	<0.03	1.97	1.27	22.5	1.43	27.5	22.6
SiO_2	41.4	56.0	53.8	0.27	41.0	57.6	57.7	42.0	55.0	0.16	0.23
K_2O	–	–	–	–	–	–	–	–	–	–	
CaO	<0.03	0.86	23.0	<0.03	0.03	0.26	0.25	5.54	24.2	0.06	<0.03
TiO_2	<0.03	0.03	0.04	<0.03	<0.03	<0.03	<0.03	<0.03	<0.03	0.06	0.04
Cr_2O_3	<0.03	0.67	1.13	30.9	<0.03	0.25	0.23	1.54	0.54	42.5	47.1
MnO	0.11	0.14	0.09	0.18	0.10	0.10	0.09	0.50	0.06	0.29	0.25
FeO	7.85	5.09	1.46	11.2	7.63	4.83	4.7	7.5	1.41	12.1	13.6
Fe_2O_3	–	–	–	1.33	–	–	–	–	–	2.04	2.03
NiO	0.44	0.11	0.04	0.07	0.42	0.11	0.07	<0.03	<0.03	0.09	0.05
Total	101.6	101.0	101.1	98.2	100.9	100.7	101.1	99.7	101.2	100.7	100.3

Table 1 (continued)

	PHN5264							PHN 2793/8B		
	Olivine	High-Al enstatite	Low-Al enstatite	Garnet	Diopside	High-Al spinel	Low-Al spinel	Garnet	Ilmenite	Rutile
Na_2O	<0.03	<0.03	<0.03	<0.03	0.86	<0.03	<0.03	<0.03	–	–
MgO	52.7	35.2	36.6	21.7	17.7	18.0	17.3	11.8	3.77	0.04
Al_2O_3	<0.03	2.76	1.34	23.3	1.8	35.9	26.3	22.1	0.49	0.51
SiO_2	41.0	57.4	58.6	42.4	54.8	0.13	0.27	39.0	<0.03	<0.03
K_2O	–	–	–	–	–	–	–	–	–	–
CaO	<0.03	0.29	0.21	4.66	24.1	0.03	<0.03	1.38	<0.03	0.03
TiO_2	<0.03	<0.03	<0.03	<0.03	0.03	<0.03	0.13	0.03	53.9	97.5
Cr_2O_3	<0.03	0.55	0.21	1.16	0.81	33.1	42.0	0.27	0.19	0.33
MnO	0.05	0.09	0.35	0.04	0.13	0.18	0.42	0.22	<0.03	
FeO	6.57	4.18	4.25	7.12	1.18	9.85	9.72	24.9	41.7	0.36
Fe_2O_3	–	–	–	–	–	1.88	3.59	–	–	–
NiO	0.45	0.1	0.08	<0.03	0.03	0.08	0.11	<0.03	<0.03	<0.03
Total	100.8	100.6	101.4	100.7	101.3	99.1	99.6	99.9	100.3	98.8

of flakes with a grain size ranging up to 3 mm. In many specimens the graphite is interstitial, but locally the flakes are fully or partially enclosed in enstatite grains (Fig. 2a). The association of graphite with enstatite in the pyroxenites is similar to that observed for the peridotites. An orthopyroxenite xenolith from Premier (FRB1399), with minor diopside and olivine, contains large (>10 mm) polycrystalline blebs of graphite as well as graphite inclusions in enstatite, together forming 10–20% of the xenolith. The high abundance of graphite in this xenolith is comparable to a lherzolite from Premier Mine containing approximately 60% graphite (Mathias et al. 1970). It is possible that there are two generations of graphite in FRB1399. Single, sub-mm euhedral blades are partially enclosed by fresh enstatite grains whereas larger, 0.5 to 2 mm graphite grains appear partially to be replacing very altered enstatite and form multicrystalline aggregates of irregular "clots". Although no fabric is observed in the silicates, both types of graphite display a high degree of preferred orientation.

Two amphibole-bearing peridotites contain several multicrystalline stacks of graphite; other periodotites contain single "stacks". Aggregates of graphite crystals have a vein-like distribution in two specimens from Jagersfontein. In pargasite-bearing garnet peridotite PHN5633, the flakes of graphite are concentrated on a flat face of the xenolith, suggesting an origin on a vein wall that localised fragmentation. In garnet lherzolite JAG 500, the graphite is concentrated in two diffuse bands (Fig. 2b), one coincident with a zone of garnet and diopside within the host harzburgitic assemblage (Field and Haggerty 1990); the second graphite band is parallel to the first, but transects coarse olivine and enstatite.

Characterisation of the graphite

X-ray analyses of the graphites indicate they are well ordered, with $d_{002} \sim 3.34$ Å and show well resolved (112) and (114) lines. Graphites from the peridotites give Raman spectra comparable to those of highly crystalline graphite from granulite-facies metamorphic terrains, where the graphite was derived either from thermal maturation of an organic precursor or precipitation from a C–O–H fluid (Pasteris and Wopenka 1991; Wopenka and Pasteris 1993; this paper, Fig. 3a, spectrum 2). Raman spectra of all the xenolith graphites analysed (Fig. 3a, spectrum 1) have well defined first- and second-order peaks, most of which are at or close to the normal peak positions, indicating continuity on the order of thousands of Angstroms within the basal plane (i.e. thousands Å $< L_a < \infty$). Such spectra are characteristic of a high-temperature origin and are distinct from those of either fine-grained graphite found in serpentinised kimberlitic olivine (Pasteris 1981, 1988) or carbon precipitated in fluid inclusions where the fluids are brought to graphite saturation at moderate temperatures and/or pressures (Fig. 3a, spectra 3 and 4).

Raman spectra of graphites from lower crustal eclogites PHN2793/8B and PHN2793/8C are similar to those of the peridotites and indicate highly crystalline graphite of high-temperature origin. The carbon isotopic composition of the graphite in PHN2793/8c is significantly lighter than the peridotites, indicative of a different origin for the carbon. The similarity of Raman spectra for graphites from crustal eclogites and peridotites indicates that, as expected, Raman spectroscopy is not capable of distinguishing isotopically different, highly crystalline graphite that may have crystallised from different reservoirs and/or carbonaceous parents. Although most of the xenolith spectra have peak positions that are normal for highly crystalline graphite (Fig. 3a), numerous graphite grains from pyroxenite JX-23, show deviations from the above spectra, with downshifting of the first- and second-order peaks that is not presently understood (Fig. 3b, spectra 2 and 3). A recent study by Everall et al. (1991) documents downshifting of the first-order Raman bands for carbon fibres and graphite in response to laser-induced heating of the sample during Raman microprobe analysis. Although the graphites from JX-23 are as highly crystalline as those from other samples in this study, the former may be more susceptible to heating – an hypothesis that will be investigated in the near future.

Thermobarometry

A principal aim of this investigation has been to evaluate the possibility of metastable crystallisation of graphite

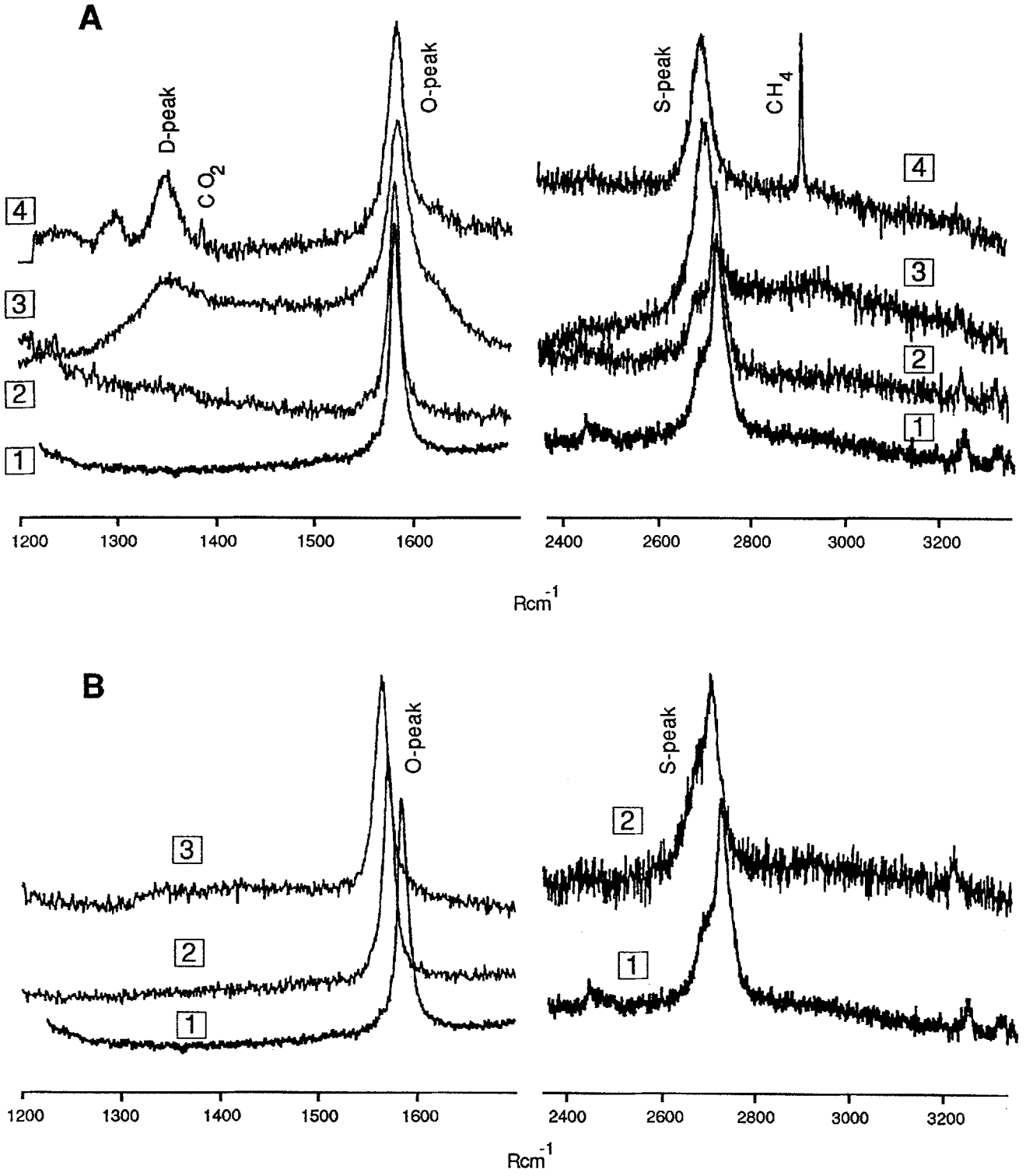

Fig. 3. **A** First-order, *left*, and second-order, *right*, Raman spectra of: *1*, graphite from spinel harzburgite sample PHN4258; 2, vein-type, granulite-facies graphite from Sri Lanka; *3*, graphite in mantle xenolith olivine from San Carlos volcanic field in Arizona, artificially induced to precipitate in CO_2 inclusion at about 1400° C and 5 kbar at an fO_2 approximating that of the iron-wustite buffer assemblage (see Pasteris and Wanamaker 1988); *4*, graphite in quartz from Colorado Front Range, artificially induced to precipitate in CO_2 inclusion at about 725° C and 2 kbar at an $fH_2 \sim 243$ bars (see Morgan et al. 1993). Note that the position and width of the first-order O-peak are almost indistinguishable between Sri Lanka and peridotitic graphites. Minor peak on the left shoulder of O-peak represents oxygen in ambient air. D-peak labelled on other first-order spectra indicates structural disorder in those phases. Second-order S-peak has well resolved shoulder only for the peridotite and Sri Lanka graphites. **B** Comparison of first-, *left*, and second-order, *right*, spectra of xenolith graphites from this study: *1*, same as spectrum 1 in Fig. 3a; *2* and *3*, graphite grains from exsolved eclogitic megacryst JX-23. Absence of D-peak in the first-order spectra indicates highly crystalline graphite. Note peak shifts from *1* 1581 cm^{-1} (normal graphite) to *2* 1571 cm^{-1} in first-order spectra and from *1* 2725 cm^{-1} to *2* 2711 cm^{-1} in second-order spectra

within the diamond stability field. Several studies document the coexistence of primary diamond and graphite in eclogite (Bobrievich et al. 1959; Sobolev 1974; Pokhilenko et al. 1982; Robinson 1979; Robinson et al. 1984) and some peridotite (Sobolev et al. 1984; Viljoen et al. in press) xenoliths. These occurrences indicate the possibility of at least limited metastability of graphite or diamond. The nature of graphite crystallisation, whether stable or metastable, is clearly relevant to an understanding of the physio-chemical process by which the graphite formed. Moreover, the possibility of graphite metastability is of practical interest in mineral thermobarometry. Occurrences of diamond and graphite in peridotite xenoliths can be used to test the methods of thermobarometry by comparison of estimated equilibration conditions with the experimentally determined diamond-graphite stability curve, provided it can be shown that the diamond and graphite have crystallised within their respective stability fields. In the past such tests have depended critically on two specimens which closely bracket the diamond-graphite curve, graphite-bearing lherzolite PHN1569 and diamond-bearing lherzolite BD2125 (Finnerty and Boyd 1984, 1987). Evidence of metastable crystallisation of graphite would obviously limit the effectiveness of such tests in evaluating thermobarometric methods.

Equilibration pressures for the graphite-bearing peridotites, calculated from the data presented in Table 1, range widely, from those characteristic of shallow mantle within the spinel-peridotite facies (<2 GPa), two well

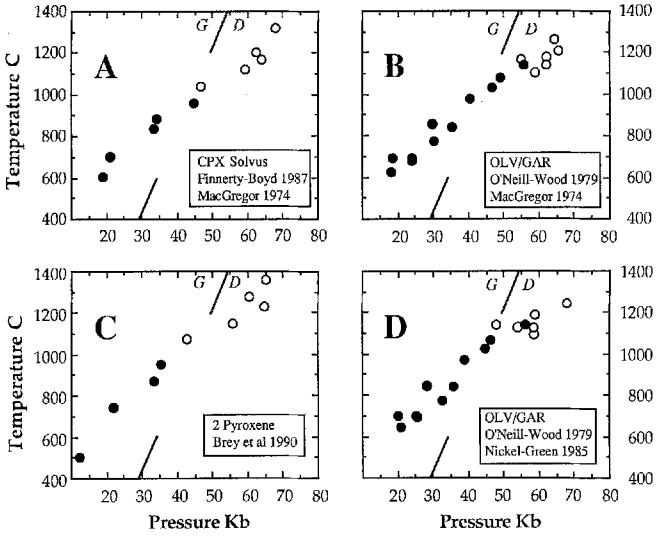

Fig. 4A–D. Temperature and pressure of equilibration for graphite-bearing peridotites, *solid circles* and diamond-bearing peridotites, *open circles* calculated using a variety of thermobarometer combinations. **A** T by the Finnerty and Boyd (1987) pyroxene solvus thermometer (FB86), P by the MacGregor (1974) barometer (MC74); **B** T by Fe–Mg olivine-garnet thermometer of O'Neill and Wood (1979), P by MC74; **C** T by the pyroxene solvus thermometer of Brey and Kohler (1990), P by the Brey et al. (1990) barometer; **d** T by O'Neill and Wood (1979), P by Nickel and Green (1985). For a discussion and references the reader is referred to Finnerty and Boyd (1987). Data for diamondiferous peridotites from Boyd and Finnerty (1980); Shee et al. (1982) and Viljoen et al. (1992)

within the garnet stability field, some close to the graphite-diamond transition (Fig. 4). Fewer points appear in plots for which temperature was calculated from the pyroxene solvus (Fig. 4a and c), because many of the graphite peridotites lack diopside. Additionally, the garnet in lherzolite PHN2265 has been completely altered to fine-grained kelyphite, thereby preventing application of thermometers based on Fe–Mg exchange between olivine-garnet and orthopyroxene-garnet.

Temperatures and pressures calculated for the graphite-bearing garnet peridotites, using a variety of thermobarometer combinations, are consistently less than those calculated for diamond-bearing peridotites (Fig. 4). The consistency of the *relative* positions of the samples in $P-T$ space is evidence that the graphite and diamond in these rocks crystallised within their respective stability fields and provides independent support for a primary, mantle origin for the graphite. Unfortunately we have not been able to analyse any peridotite containing both diamond and graphite. A point for a graphite peridotite overlaps a point for a diamond peridotite in only one plot (Fig. 4d); these two samples have a more consistent relationship in Fig. 4b. The discrepancy in Fig. 4d therefore appears more likely to be due to a minor failure of thermobarometry than to metastable crystallisation. Having shown that equilibration pressures and temperatures for the peridotites are consistent with the *relative* stability relationships for graphite and diamond (i.e. there is no significant metastability of either phase in the samples studied) we can evaluate the accuracy of the thermobarometers with respect to the experimentally determined diamond-graphite transition. For this comparison we have employed the diamond-graphite transition curve determined by Kennedy and Kennedy (1976). Their curve was obtained using a modified piston-cylinder apparatus and the pressure and temperature measurements have a greater accuracy than those of earlier experiments carried out with a belt apparatus (Bundy et al. 1961).

The transition in temperature and depth from graphite- to diamond-bearing peridotites that is illustrated by the plots in Fig. 4 closely approximates the graphite-diamond equilibrium boundary determined by independent experiment (Kennedy and Kennedy 1976). This relationship represents a significant success for peridotite thermobarometry. Our results indicate that equilibration conditions estimated using the diopside solvus (e.g. Finnerty and Boyd 1987) combined with the Al-isopleths of MacGregor (1974) are in best agreement with the experimentally determined diamond-graphite curve but other combinations are not significantly different. Furthermore, the pressure-temperature estimates for the graphite-bearing peridotites confirm their origin within the lithospheric mantle.

Only one of the four graphite-bearing garnet lherzolites from Premier (FRB1350) contains sufficiently homogeneous garnet and pyroxene to permit quantitative estimate of the depth of origin. This rock appears to have equilibrated at a depth of 100 km or less, well within the graphite stability field. The other three lherzolites contain fine-grained garnets with a predominantly inter-

Table 2. Carbon isotope compositions of graphite in peridotite, pyroxenite and eclogite xenoliths and megacrysts. Note that PHN 2793 is of lower crustal origin. Letters in parentheses indicate graphite samples extracted from different places within one xenolith fragment. Carbon isotope data were obtained at the Open University and The Geophysical Laboratory using standard techniques described in Pearson et al. (1991a) and Bebout and Fogel (1990)

Sample	Locality	Lithology	δ^{13}C‰ PDB
Peridotites			
E-8	Thaba Putsoa	Garnet harzburgite	−9.8
PHN 1555a	Mothae	Harzburgite	−12.3
PHN 1569	Thaba Putsoa	Garnet lherzolite	−6.7
PHN 2492	Kao No. 2	Low-Ca Garnet harzburgite	−5.8
PHN 4258	Letseng-la-Terai	Spinel harzburgite	−7.1
PHN 5633(a)	Jagersfontein	Pargasite bearing Garnet harzburgite	−6.9
PHN 5633(c)			−6.3
PHN 5633(d)			−7.9
JAG 84-500(a)	Jagersfontein	Graphite associated with	−5.4
JAG 84-500(b)	Jagersfontein	garnet clinopyroxenite in garnet harzburgite	−4.8
JAG 84-500(A)	Jagersfontein		−4.0
JAG 84-500(B)	Jagersfontein		−5.2
K7-232	Jagersfontein	Garnet harzburgite	−6.9
JAG 89-5	Jagersfontein	Garnet harzburgite	−3.8
FRB 888	Bulfontein	Garnet harzburgite	−5.0
UV404/86	Udachnaya	Garnet lherzolite	−6.5
FRB930/B2	Premier	Spinel lherzolite	−7.0
PHN 5235	Premier	Garnet-spinel lherzolite	−6.9
PHN 5264	Premier	Garnet-spinel lherzolite	−9.3
Megacrysts, eclogites and pyroxenites			
JX-23	Jagersfontein	Pyroxenite	−6.8
JAG 89-10	Jagersfontein	Orthopyroxene megacryst	−7.2
JEC 89-G	Jagersfontein	Eclogite	−5.9
FRB 1384	Premier	Orthopyroxenite	−13.6
FRB 1399(a)	Premier	Orthopyroxenite	−18.9
FRB 1399(b)	Premier	Orthopyroxenite	−19.4
O8/89	Obnazhennaya	Orthopyroxenite	−9.3
PHN2793/8C	Kao	Ilmenite-rutile eclogite	−17.1

stitial habit (Appendix 2), suggesting late-stage crystallisation, perhaps by cooling across the garnet-in boundary. Diopside in the three inhomogeneous Premier peridotites is Ca-rich, indicating a low equilibration temperature, and the orthopyroxene and spinel are Al-rich in comparison to those in most garnet peridotite xenoliths, suggesting a relatively shallow mantle origin. The chemical inhomogeneities in the minerals in these Premier peridotites are similar to those found in Kaapvaal spinel peridotites and appear to correlate with low ambient temperatures in the shallow mantle.

The combination of two-pyroxene thermometers, with either the barometer of Brey and Kohler (1990) or MacGregor's (1974) Al_2O_3 isopleths in the MAS system give anomalously low equilibration pressures for one of the garnet peridotites (JAG-244; ~1.2 GPa and 0.1 GPa respectively). More reasonable pressures of about 2.2–2.3 GPa are obtained using an Fe−Mg garnet-olivine thermometer (e.g. O'Neill and Wood 1979) with the barometer of MacGregor (1974), Nickel and Green (1985), or Brey and Kohler (1990, not shown). The irregular results obtained by using the two-pyroxene thermometers for this specimen are probably a result of insensitivity of the pyroxene solvus at low temperatures.

Carbon isotopes

Peridotites

Carbon isotopic compositions of graphite from the peridotites analysed in this study vary from $\delta^{13}C = -12.3$ to −3.8‰ (Table 2). This range encompasses previously reported values for graphite in peridotites (Schulze and Valley 1991; Viljoen et al. in press). The total population has a primary mode between −6 and −7‰, co-incident with a mean of −6.7‰, $\sigma = 2.1$ ($n = 22$), as shown in Fig. 5a. The isotopic variation in peridotite-derived graphite envelops the range for diamonds in diamondiferous peridotites (−7.0 to −2.8‰, $n = 18$). Diamonds in peridotite xenoliths show a mode between −3 and −4‰, with a mean of −4.0, $\sigma = 1.0$ (Fig. 5b). Although the mean for the xenolith diamonds is almost 3‰ heavier than for graphite from peridotites, the two means are within one standard deviation of each other and thus are not significantly different. The isotopic range of diamonds from peridotites is only half that of the graphite; no diamonds extend to the isotopically light values (< −9‰) shown by some graphites. The modes of both graphite and diamond from peridotite xenoliths differ slightly from the mode of between −5 and −6‰ for a much larger population of P-type diamonds (see Gur-

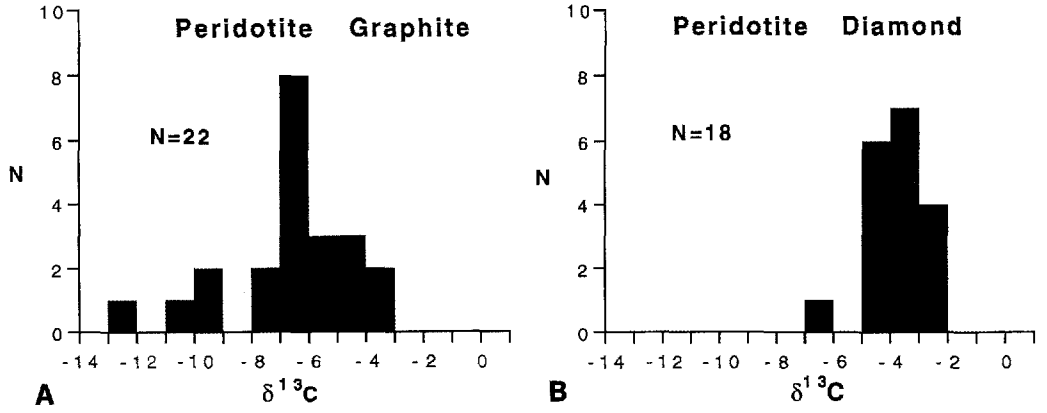

Fig. 5. A Histogram of carbon isotope distribution for graphite from peridotite xenoliths, included are data for one specimen from Schulze and Valley (1991) and two from Viljoen et al. (in press). **B** Histogram of carbon isotope distribution for diamond from peridotite xenoliths, data from Deines et al. (1984), Jaques et al. (1990), Viljoen et al. (1992), Viljoen et al. (in press)

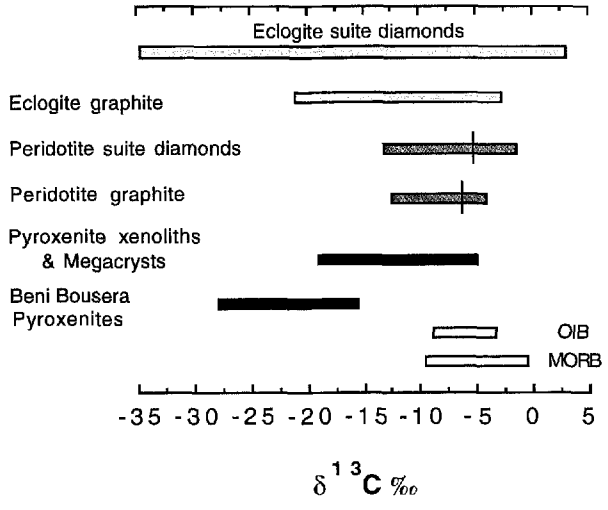

Fig. 6. Carbon isotope variation of graphite and diamond from peridotite and eclogite suite assemblages compared to that for graphite in pyroxenite xenoliths and megacrysts (this study), graphite in pyroxenite layers in the Beni Bousera peridotite massif (Pearson et al. 1991a), MORB and OIB (Taylor 1986; Exley et al. 1986). The *vertical lines* across the peridotite suite diamonds and peridotite graphite ranges represent the modes for the distribution

ney 1991 for recent compilation). However, the xenolith populations are small and the total isotopic range for graphite in xenoliths is similar to that for P-type diamonds (Fig. 6). There is no consistent relationship between equilibration pressures of the peridotites and carbon isotopic composition of their graphite, as suggested for diamonds by Deines et al. (1991).

Three graphite flakes extracted from within 3 cm of each other in the amphibole-bearing peridotite PHN5633 show a total isotopic variation of 1.6‰ and four different flakes of the "vein-like" graphite from garnet lherzolite JAG500 show a variation of 1.4‰. Graphite from pyroxenite FRB1399 shows a 5.6‰ variation from flakes several cm apart. Galimov et al. (1989) reported $\delta^{13}C$ values of -7.6 to -8.1‰ in four separate flakes from a pyroxenite xenolith from the Udachnaya kimberlite. Such small-scale carbon isotope variation has also been described by Rumble and Hoering (1986) for graphite veins in regionally metamorphosed crustal rocks in New Hampshire, U.S.A. These authors attributed the variations in isotopic composition to differences in graphite precipitation conditions caused by mixing of isotopically different fluids, mixing of fluids with different CO_2/CH_4 ratios and/or changing temperature. Similar processes operating within the mantle could have caused some of the small-scale isotopic variation observed in the xenoliths studied here, i.e. progressive isotopic evolution of C-bearing fluid moving through fractures in the lithosphere.

Pyroxenites and eclogites

Graphite from the Obnazhennaya pyroxenite, O8/89 has a $\delta^{13}C$ value within the range of the peridotites (-9.3‰) but that from the two pyroxenites from Premier is more depleted in ^{13}C than any graphite from a peridotite (-18.9 to -13.5‰ in FRB1399 and -19.4‰ in FRB1384). The mean for the three pyroxenites studied here is -15.3‰, $\sigma = 4.8$. Galimov et al. (1989) reported $\delta^{13}C$ values of graphite in metasomatised websterites from Siberian kimberlites ranging from -7.4 to -22.7‰. Isotopically light graphite (-27 to -16‰) has also been reported from pyroxenite layers within the Beni Bousera orogenic peridotite massif (Pearson et al. 1991; Fig. 6). It thus appears that graphite from pyroxenites is more isotopically variable than peridotitic graphite. Graphite from the one mantle eclogite analysed in this study has a $\delta^{13}C$ value of -5.9‰, similar to the mean value of -6.2‰ ($\sigma = 2.6$‰, $n = 47$) for graphite in eclogite xenoliths analysed by Deines et al. (1987, 1991) and Schulze et al. (1991). The range for all graphite from eclogites ($\delta^{13}C = -20.3$ to -2.8‰) is more variable than that of the peridotites (Fig. 6). The wider isotopic variation shown by graphite from eclogites and pyroxenites is consistent with the more variable isotopic compositions of E-type diamonds compared to P-type diamonds (Fig. 6). Graphite in the exsolved enstatite megacryst from Jagersfontein lies within the range for peridotites and pyroxenites (Fig. 4a; $\delta^{13}C = -7.2$).

The isotopic composition of graphite in the lower crustal eclogite, PHN2793/8C, from Kao is depleted in ^{13}C (−17.1‰), comparable to some graphite from other lower crustal lithologies (e.g. Pearson et al. 1991 a) and may represent metamorphosed organic matter.

Discussion

Pyroxenites and eclogites

The carbon isotopic range of graphite in the pyroxenites and eclogite is much greater than for graphites in peridotites (Fig. 6). Graphite in these rocks is generally sparsely distributed, as in the peridotites, except for an orthopyroxenite from Premier, FRB1399, which contains between 10 and 20 vol.% graphite. This xenolith petrographically resembles the pyroxenite cumulates from the Bushveld intrusion. The Premier kimberlite erupted within the outcrop ring of the Bushveld intrusion and thus might have incorporated inclusions from this body. However, graphite in the Bushveld samples is commonly associated with hydrous silicates such as amphibole and phlogopite (Ballhaus and Stumpfl 1985), whereas the primary minerals in FRB1399 are anhydrous. Much of the graphite in FRB1399 appears to show a replacement texture after very altered enstatite and appears to be texturally younger than the more euhedral graphite partially enclosed by fresh enstatite grains. The very altered nature of most of the enstatite in this xenolith prevents estimation of its depth of origin. It is significant that graphite from this xenolith has the lightest carbon isotope composition of the those analysed ($\delta^{13}C = -18.9$ to -19.4‰), similar to the lower crustal eclogite from Kao (−17.1‰). The isotopic composition of FRB1399 is in the range found for graphite in orthopyroxene-rich pyroxenite cumulates of lower crustal origin from the Eggèrè region of the Sahara (−24.6 to −14.4‰; Pineau et al. 1987). Hence, FRB1399 and possibly the other pyroxenite from Premier FRB1384) with comparably light carbon isotopes (−13.6‰) may be derived from a lower crustal ultramafic intrusion. In contrast, the orthopyroxenite from Obnazhennaya, O8/89 shows petrographic features such as high-temperature exsolution of garnet and diopside from enstatite that are consistent with a mantle derivation (Appendix 2). A $\delta^{13}C$ value of −9.3‰ for the graphite from O8/89 is heavier than the other pyroxenites and within the range of "typical mantle carbon" as characterized by MORB and OIB (Fig. 6).

Peridotites

Graphite crystallisation. The occurrence of multiple graphite flakes of vein-like form in several Jagersfontein peridotites suggests a metasomatic origin, as advocated by Field and Haggerty (1990). Deposition of graphite in the peridotites could have occurred from high-temperature carbonaceous fluids, slightly undersaturated with respect to graphite, that underwent cooling during flow through fractures. C−H−O-bearing mantle fluids in contact with peridotite are likely to have high dihedral angles and high interfacial energies which prevent them from forming three-dimensionally interconnecting networks along grain boundaries (Watson et al. 1990). Such fluids favour channelised infiltration along fractures rather than pervasive penetration of solid peridotite along grain boundaries. Experiments involving the infiltration of CO_2 into synthetic dunite (Brenan and Watson 1990) suggest that fluid-driven crack propagation is possible in mantle environments. Hence, native carbon may crystallise predominantly in restricted regions close to fractures opened by supercritical fluids infiltrating the lithosphere. Such behaviour is compatible with the localised, vein-like distribution of graphite in some of the peridotite xenoliths and may account for the overall scarcity of graphite (and diamond) in xenoliths. Single graphite flakes or solitary stacks of flakes found within some peridotites may represent local precipitation within an ephemeral crack that later anneals.

The reason for the association of graphite with enstatite grains in numerous peridotite xenoliths and in enstatite-rich pyroxenites is not clear but could be related to surface energies. It is also relevant to note that in mantle-derived rocks there is a marked association of fluid inclusions with pyroxenes (Pasteris 1987). The association of trapped fluids with pyroxenes is supported by the high concentration of CO_2 released from pyroxenes relative to other mantle minerals during step-heating for isotopic analysis (Mattey et al. 1989). The more brittle response of pyroxene compared to olivine during high-temperature deformation may allow fracturing and ingress of fluids which may be trapped either as fluid inclusions or may precipitate graphite in some circumstances.

Isotopic constraints. There are several possible explanations for the isotopic range of the graphites. Schulze (1986) has argued that lithospheric peridotites containing subcalcic high-chrome pyrope garnets are the products of subduction of serpentinised abyssal peridotites. Subduction of oceanic peridotites may entrain marine carbonate and organic matter which could re-crystallise or be re-mobilised and deposited as graphite or diamond (Schulze 1986; Schulze and Valley 1991). The compositions of most peridotites forming the lithospheric keel beneath the Kaapvaal craton differ in composition from oceanic peridotites and may be residues of partial melt extraction at depth during the Archaean (Boyd 1989; Boyd et al. 1993; Walker et a. 1989; Pearson et al. 1991 b; Canil 1992) with subsequent modification by metasomatic processes. The subduction hypothesis of Schulze and Valley (1991) appears improbable because of these compositional differences (Boyd et al. 1993). Other mechanisms for generating isotopic variation in the peridotite graphite include reduction-oxidation reactions of carbonaceous fluids which result in fractionation of carbon isotopes between various carbon-bearing phases and species, formation from isotopically variable fluids emanating from a heterogeneous source region, or a combination of these mechanisms.

The similarity in carbon isotopic compositions between graphite in peridotites and P-type diamonds suggests a genetic link between the two forms of carbon. The modes of the peridotite graphite and P-type diamonds are within 1‰, their isotopic ranges are similar (−12.3 to −3.8‰ and −13 to −1‰ respectively, Fig. 6) and less than 10% of both populations lie outside the range of −10 to −2‰. Furthermore, these ranges encompass the isotopic compositions of CO_2 included in minerals from peridotite xenoliths from post-Archaean mantle (Nadeau et al. 1990). Theoretical CO_2-diamond-graphite fractionation factors are such that both diamond and graphite are depleted in ^{13}C relative to a CO_2 phase (Bottinga 1969). Additionally graphite is slightly depleted in ^{13}C with respect to diamond. At the ambient temperatures of the lithospheric mantle (>800° C), these fractionation factors are less than 2‰. If graphite in peridotites crystallises from fluids genetically related to those that crystallised diamond at greater depth, at the base of the lithosphere, and if the fluids fractionate during flow through the lithosphere, then the magnitude of the calculated fractionation factors is probably adequate to account for minor differences in the isotopic character of the different peridotitic carbon populations. Theoretical calculations by Deines (1980) indicate that fractionation induced by mixing of fluids with differing speciation together with cooling can result in isotopic variations of at least 5‰. Moreover, there is the possibility that some peridotite assemblages have equilibrated with carbonate at some stage in their history (Canil 1990; Boyd et al. 1993), further complicating isotopic fractionation. Hence, we conclude that the fluids that precipitate graphite and diamond in the lithosphere probably share the same source.

The modes and overall isotopic ranges for graphite, diamond and CO_2 in peridotite are very similar to the those of carbon in MORBs and OIBs (Fig. 6). This suggests that the source of the peridotitic carbon now present in the lithosphere may have been fluids derived from the convecting mantle. S.R. Boyd et al. (1992) propose that the worldwide uniformity of carbon and nitrogen isotope distributions in MORB-OIB magmas and in the coats of coated diamonds is the result of an isotopically uniform source of volatile-rich fluids beneath the lithosphere. We suggest that the carbon associated with peridotitic lithologies in the cool, non-convecting lithospheric mantle is derived from fluids emanating from the degassing asthenosphere which cool and crystallise graphite or diamond depending on depth. The slightly wider isotopic range for graphite compared to diamonds in peridotites may be due to the shallower crystallisation of graphite, allowing more opportunity for isotopic fractionation of the carbonaceous fluid.

Tectonic association. One constraint on the origin of carbon in the lithospheric mantle that must be addressed is its almost exclusive restriction to Archaean subcratonic lithosphere. This tectonic restriction suggests that the genesis of these two forms of carbon is closely related. It also indicates that either the physio-chemical conditions prevailing in cratonic lithospheric roots are more conducive to the stabilisation of native carbon than elsewhere, or that the source of the carbon is uniquely beneath or within cratons. The f_{O_2} conditions recorded in many mantle xenoliths indicate that carbon-fluid equilibria may be important in controlling the oxidation state of the mantle (Blundy et al. 1991). However, Wood (1991) emphasises that in most cases mantle f_{O_2} is probably controlled by the interplay of carbon-fluid and $Fe^{2+}-Fe^{3+}$ solid-solid equilibria. The presence of elemental carbon in mantle assemblages, as either graphite or diamond, is not in itself indicative of exceptionally reduced conditions, only that the assemblage was at, or below the CCO (carbon-CO-CO_2) buffer (e.g. Woermann and Rosenhauer 1985). The CCO buffer is much more pressure sensitive than the typical solid-solid f_{O_2} buffer. Thus, along most oceanic and continental geotherms, carbon-fluid buffered equilibria are close to the FMQ (fayalite-magnetite-quartz) buffer (Blundy et al. 1991), effectively providing an upper limit for f_{O_2} in graphite/diamond-bearing assemblages. Oxygen fugacity estimates for many non-cratonic-continentally derived peridotite xenoliths (e.g. those from Kilbourne Hole and San Carlos) and those for oceanic peridotites are close to or below the stability limit of elemental carbon as defined by the CCO buffer (Blundy et al. 1991). The f_{O_2} estimates of these samples range as low as 2.3 log units below the FMQ buffer and thus overlap estimates for cratonic mantle (Luth et al. 1990). These observations indicate that the restriction of both diamond and graphite to peridotites from the cratonic lithosphere is unlikely to be due to unique f_{O_2} conditions in cratonic lithospheric mantle. Possibly the sources of fluids capable of precipitating elemental carbon are localised in some way beneath cratons. Subduction cannot in itself be the answer because peridotite xenoliths derived from the mantle wedge overlying Cenozoic subduction zones, such as those from western North America, do not contain primary graphite.

Brey et al. (1991) have shown that the solubility of CO_2 in kimberlitic liquids greatly decreases at pressures from 5 to 3 GPa such that a kimberlite ascending from below may degas large amounts of CO_2 on reaching the base of the cratonic lithosphere. Such a magma might eventually precipitate carbon under favourable f_{O_2} conditions (D. Canil, personal communication 1993). However, there are many kimberlites that have erupted through the lithosphere off the craton in southern Africa, in Namibia, East Griqualand and in the Karoo, south of the craton. As yet no graphite has been found in xenoliths from these areas.

The overlap of physio-chemical conditions prevailing in cratonic and non-cratonic lithosphere suggests that the concentration of carbon in cratons is most likely to have resulted from a process localised by cratons, or a process that was operative during the ancient stabilisation of cratons and their lithosphere. Pollack (1986) has suggested that cratons may originate by localisation of extensive volatile degassing from the early mantle, mechanically stiffening the mantle and forming the chemically buoyant lithosphere. Similarly, Taylor and Green (1989) suggest that redox interactions between

deep mantle-derived, reduced, CH_4-rich fluids (f_{O_2} < iron-wüstite) and oxidised regions of the pre-cratonic upper mantle (f_{O_2} ~ magnetite-wüstite-FMQ) resulted in a progressive increase in f_{H_2O} in the fluid phase. This process eventually caused partial melting leading to stabilisation of depleted lithosphere, accompanied by diamond or graphite precipitation. In their model, a CH_4-rich fluid phase may have expanded the olivine phase field relative to enstatite, leading to the generation of enstatite-rich residua (Taylor and Green 1989). This is consistent with the enstatite-rich nature of the Kaapvaal lithospheric mantle compared to oceanic mantle (Boyd 1989). It is not consistent, however, with the occurrences of P-type diamonds in the Siberian craton where the predominant host rocks are megacrystalline dunites.

A model involving generation of the carbon in lithospheric peridotites via "redox melting" during craton formation requires that graphite and diamond in lithospheric peridotites be as old as the cratonic lithosphere itself. The Sm–Nd and Rb–Sr isotope systematics of diamond inclusions indicate that: (1) at the time of diamond crystallisation, garnets in the host peridotites had experienced light rare earth element (LREE) enrichment, subsequent to melt depletion; (2) this enrichment possibly occurred several hundred million years prior to diamond crystallisation (Richardson et al. 1984). Hence, it appears that some southern African P-type diamonds crystallised after the formation of the garnets that they enclose. Additionally, high resolution ion microprobe techniques have recently revealed that some diamonds grow in multiple stages, over periods of up to 2 Ga (Rudnick et al. 1992) and over temperature intervals as large as 400° C (Griffin et al. 1993). Moreover, isotopic studies indicate that diamonds crystallised within eclogites and pyroxenites during the Proterozoic (Richardson 1986; Smith et al. 1991), possibly associated with later subduction events. These data indicate that carbon-bearing fluids/melts have infiltrated the lithosphere over considerable periods of time following its stabilisation. It should be noted that although the Sr isotope data for the Kaapvaal diamond inclusions studied by Richardson et al. (1984) suggest the possible formation of harzburgitic garnets up to 200 Ma before diamond crystallisation, the ages of the diamonds are close to the likely age of stabilisation of the Kaapvaal lithospheric mantle (Pearson et al. 1993). Thus, some lithospheric carbon appears to have crystallised close to the formation age of the lithosphere itself allowing a link between lithospheric stabilisation and carbon crystallisation.

Unfortunately, at present we have no means of dating graphite crystallisation. However, the vein-like distribution of graphite in some samples examined in this study indicate subsolidus crystallisation from an infiltrating fluid phase. Other peridotites containing single flakes of graphite may have been produced during melting.

In summary, diamond and graphite appear to be concentrated in the mantle lithosphere beneath cratons. Radiogenic isotope systematics of diamond inclusions suggest that diamond crystallisation was not directly related to the melting events that formed lithospheric peridotites. However, some diamond (and graphite ?) crystallisation occurred within the time span associated with the stabilisation of the lithospheric mantle (Pearson et al. 1993). The restriction of graphite and diamond to within cratonic mantle remains incompletely understood.

Acknowledgments. We thank M. Fogel and D. Rumble for use of stable isotope facilities at The Geophysical Laboratory. Generous laboratory assistance and advice from P. Koch and G. Bebout is particularly appreciated. D.P. Mattey is thanked for checking some of the results. Financial support for this investigation was provided by the National Science Foundation through grants EAR-9105017 and EAR-8708196 to F.R.B. and S.E.H. through NSF grant EAR911651. Acknowledgment is made to the donors of the Petroleum Research Fund (grant no. 23832-AC2-2 to J.D.P), administered by the American Chemical Society, for partial support of this research. We thank Craig Schiffries, Doug Rumble and Nick Sobolev for discussions and comments. Stuart Boyd and Dante Canil provided two very constructive reviews.

Appendix 1

Documentation of X-ray and Raman spectroscopy

X-ray diffraction measurements were made using a Debye-Scherrer powder camera with the Straumanis mounting arrangement. To avoid preferred orientation effects several crystals of graphite were ground with a small amount of quartz.

One to six grains of graphite from each of the xenolith samples PHN 1555a, PHN 4258, JAG 89-5, JAG 89-10, JX-23, PHN2793/8B and PHN2793/8c were analysed by Raman microsampling spectroscopy, using an Instruments SA (Jobin-Yvon) RAMANOR U-1000 equipped with an Olympus BH-2 research-grade microscope. This is a scanning instrument in which single-channel detection is provided by a thermoelectrically cooled RCA C31034 photomultiplier tube. The grains were placed on a glass slide and irradiated with the 514.5 nm line of a 5-Watt Ar-ion laser (Coherent Innova 90-5). The laser was focused with a Nachet 40X objective (numerical aperture = 0.75), providing about 15 mW laser power at the sample surface; the beam was approximately perpendicular to the basal plane of the graphite. The spectral regions 1200–1700 and 2350–3350 R cm^{-1} were scanned at a resolution of about 5 cm^{-1}. The spectral step size was 1 cm^{-1}, and the counting time was 10 seconds per step. In some cases, it was necessary to sum multiple scans in order to obtain an appropriate signal-to-noise ratio.

Appendix 2

Petrography of graphite-bearing ultramafics

E-8 Thaba Putsoa. Coarse harzburgite with sparse, lilac coloured garnet and relatively abundant graphite in discrete flakes between grains of olivine and enstatite. Graphite forms approximately 0.03 wt% of the rock. Rounded granules of chromite are included in olivine.

PHN 1555a Thaba Putsoa. Coarse spinel harzburgite, with several 1–2 mm diameter graphite clusters interstitial between weathered olivine and enstatite crystals. Graphite crystallites within clusters are euhedral.

PHN 1569 Thaba Putsoa. Coarse, fresh-appearing garnet lherzolite with olivine and enstatite grains ranging up to 5 mm. Smaller,

scattered garnets exhibit extensive reaction to kelyphite. Grains of diopside, 1 mm or less in diameter, are dispersed, commonly in association with garnet. Graphite is widely dispersed in crystals that are one to several tenths of a mm in maximum dimension.

PHN 2265 Kao. Coarse lherzolite, fresh-appearing with slightly strained olivine ranging up to 0.5 cm. Garnet has been wholly altered to kelyphite. Single mm size graphite crystal stack.

PHN 2472 Kao. Low-Ca garnet harzburgite with dispersed multicrystalline stacks of graphite. Texture is coarse but both olivine and enstatite have markedly undulose extinction. Irregularly shaped garnets are rimmed with kelyphite and discontinuous mantles of strongly pleochroic phlogopite.

PHN 2793-8B Bellsbank, N. pipe. Chip (1 cm) that is rich in coarse (1–3 mm), pale pink garnet interspersed with pale gray alteration products, graphite flakes (1 mm), ilmenite and rutile. Some graphites are euhedral and partially included in garnet, suggesting synchronous, high-temperature growth. The garnet is richer in Fe than pyropes from peridotites and has less Ca than most garnets from mantle eclogites. Its composition is similar to some garnets in gneisses and granulites (Deer et al. 1982, p 541) and therefore the rock may be of crustal origin.

PHN 2826B Lighobong, NW Blow. Low-Ca garnet harzburgite. Texture is coarse with olivine grains ranging up to 1 cm. Minor strain features include undulose extinction and sparse kink bands. Garnets with irregular shapes have inhomogeneities in Ca and Cr within and between grains; ranges are 2.44–4.12 Cr_2O_3 and 2.73–3.21 CaO, wt%. There are sparse grains of red-brown, Al-rich spinel and widely dispersed crystals of graphite.

PHN 4258 Letseng-la-Terai. Coarse spinel-facies peridotite with fresh-appearing, little strained olivine and enstatite in grains ranging up to 1 cm. The enstatite contains 1.66 wt% Al_2O_3, indicative of spinel rather than garnet facies. There are numerous scattered, irregularly shaped grains of red-brown, aluminous spinel. Crystals of graphite are sparsely distributed.

PHN 5633 Jagersfontein. Coarse, pargasite-bearing garnet peridotite with multiple platelets of graphite concentrated on a planar face of the xenolith. The planar face may be one wall of a broken vein. Several of the graphite flakes, up to 1 mm long, are included within orthopyroxene porphyroclasts. Olivine crystals range up to 6 mm and exhibit little sign of strain. Pargasite has partially replaced orthopyroxene and there is much fine-grained interstitial mica. Granules of reddish spinel are included in olivine and garnet.

FRB 888 Bultfontein. Coarse garnet harzburgite containing a flake of graphite 0.5 mm in diameter. Olivine and enstatite ranging to over 0.5 cm are fresh appearing, but exhibit minor strain. Garnets have extremely irregular contorted grain boundaries partially enclosing enstatite. They are Ca saturated, but strongly zoned with margins enriched in Ca and Cr. The centre to edge compositional variation in one grain is 4.32–4.67 CaO and 3.86–4.95 Cr_2O_3, wt%. There are sparse grains of primary chromite. This specimen is from the Sampson collection at Princeton and has the original number 7429.

FRB 1399 Premier. Orthopyroxenite nodule 5 cm in maximum dimension that contains 10–20% graphite. Two types of graphite are evident, irregular, multicrystalline clots up to 5 mm, associated with, or partially replacive of very altered enstatite. More euhedral, sub-mm blades of graphite are partially enclosed by relatively fresh enstatite. All graphite crystals have a strong preferred orientation that is not evident in the silicate grains. Orthopyroxene grains ranging up to 1 cm are entirely altered to serpentine that is relatively rich in Fe and Al. Accessory diopside and olivine are dispersed as grains ranging up to 1 mm. The diopside is markedly inhomogenous in Al, Na, Ti and Cr.

JAG 89-5 Jagersfontein. Coarse garnet lherzolite with approximately 50 vol.% enstatite. The olivine is unstrained and ranges to 1 cm. The enstatite contains abundant lamellae of garnet and spinel with less common diopside. Graphite occurs as scarce multicrystalline stacks. The diopside and garnet also occur as discrete grains interstitial to olivine and enstatite.

K7-232 Jagersfontein. Coarse (3–5 mm) garnet lherzolite with numerous dispersed flakes of graphite ranging up to 2 mm. The graphite cross-cuts olivine and enstatite grain boundaries and some flakes are mantled with fine-grained phlogopite. Garnet has an unusual elongate habit and spinel is clustered in rounded, irregularly shaped grains. There is a single small (0.2 mm) grain of diopside included in enstatite. The diopside is not suitable for thermobarometry because of severe inhomogeneities.

K7-244 Jagersfontein. Coarse garnet lherzolite with a grain size ranging up to 1 cm. Diopside and garnet are relatively poor in Cr and some diopside is intergrown with and included in enstatite. The xenolith contains many platelets of graphite that are a few tenths of a mm in diameter. These appear to be preferentially included in garnet.

JAG 84-292 Jagersfontein. Amphibole-bearing garnet harzburgite with coarse olivine, ranging to 6 mm, surrounding clusters of equally coarse enstatite intergrown with more fine-grained garnet and spinel. The enstatite contains abundant lamellae of diopside and spinel. Garnet grains mantle enstatite. Pargasite is spatially associated with enstatite both as intergrowths and interstitial grains. Graphite predominantly forms interstitial platelets ranging to 1.5 mm.

JAG 84-500 Jagersfontein. Coarse harzburgite transected by a centimeter-wide band that is rich in diopside and garnet. The xenolith contains two parallel bands of graphite crystals (Fig. 2b), one intergrown with the diopside and garnet and the other isolated in olivine and enstatite. Within these bands there are numerous graphite crystals, ranging to 3 mm, some interstitial and others included in garnet or olivine and enstatite.

JEC 89G Jagersfontein. Coarse equigranular eclogite with accessory rutile, associated ilmenite and sparse polymineralic sulphides. Euhedral to subhedral and blocky graphite (1–3 mm × 2 mm) crystals are typically at garnet and clinopyroxene grain boundaries but locally penetrate clinopyroxene and rarely garnet. Graphite crystals exhibit wavy optical extinction and unusual sigmoidal pods of recrystalised graphite within larger optically homogenous grains.

JX-23 Jagersfontein. A pyroxenite of approximately equal proportions of ortho- and clinopyroxene, a trace of olivine and attached kimberlite. Graphite is in coarse flakes and is confined to a prominent veinlet (0.5–1 mm wide and 2 cm in length) in the orthopyroxene segment of the xenolith. Graphite is not identified in the kimberlite.

JAG 89-10 Jagersfontein. A complex pyroxene megacryst composed of clinopyroxene and finely exsolved orthopyroxene, and an orthopyroxene-dominant part of the xenolith with coarsely exsolved clinopyroxene and garnet. Thin (10–20 μm) filamental graphite is present along clinopyroxene-orthopyroxene exsolution contacts, and coarser (0.5–1 mm) platelets of graphite are confined to the coarser grained silicate assemblage along exsolution interfaces. Kimberlite coats a part of the xenolith and some graphite appears to be related to the kimberlite.

UV 404/86 Udachnaya. Peridotite chip with the mineral assemblage of a garnet lherzolite but with marked variations in grain size and heterogeneities in the distribution of minerals. An ultra coarse grain of orthopyroxene (3 cm) is bordered by more fine-grained orthopyroxene and olivine together with a crude vein of diopside flanked by garnet. Garnet has exsolved from the coarse orthopy-

roxene in 0.1 mm lamellae that parallel the cleavage trace as well as in elongate blebs that are predominantly perpendicular to cleavage. The latter may have been localised by kink bands and subsequently annealed. Flakes of graphite are included in the orthopyroxene, up to 0.5 mm diameter. Fine-grained red-brown spinel is spatially associated with diopside and has also crystallised in symplectites.

O8/89 Obnazhennaya. High-temperature orthopyroxenite with garnet and Cr-rich clinopyroxene exsolved from the enstatite; minor olivine also present. Two multicrystalline stacks of graphite partially included within coarse enstatite crystals.

FRB 930/B2 Premier. Coarse garnet lherzolite with olivine and relatively abundant enstatite ranging up to 6 mm. The enstatite has fine exsolution, like that in many Kaapvaal spinel peridotites. Sparse, fine-grained interstitial garnet is clustered with spinel and diopside. Red spinel occurs in granules with irregular shapes as well as in symplectites. The alumina content of the enstatite varies from 1.10 to 1.57 wt% and the spinel exhibits moderate inhomogeneities in Mg, Fe, Al and Cr. Analyses for these minerals in Table 1 are averages. There are four multicrystalline aggregates of graphite of interstitial habit.

FRB1350 Premier. Fresh appearing, large ($20 \times 14 \times 5.5$ cm) garnet-spinel lherzolite with ultra coarse olivine that exhibits little strain. Relatively abundant grains of diopside and garnet (~ 2 mm) that are clustered and possibly exsolved from the enstatite. Scarce, primary-appearing granules of spinel (< 0.2 mm) are dark red to opaque. Graphite flakes up to 1 mm long are widely dispersed and interstitial.

FRB1384 Premier. Ultra coarse, little altered spinel websterite/orthopyroxenite, with enstatite grains ranging up to 2 cm. Irregular small grains of diopside and dark red spinel are predominantly interstitial. The enstatite has exsolved diopside on a fine scale. Accessory olivine is present in patches of serpentine. Three 0.6 mm interstitial aggregates of graphite crystallites.

PHN5235 Premier. Coarse garnet-spinel lherzolite with slightly strained olivine grains ranging to 6 mm. Abundant enstatite crystals exhibiting fine exsolution are mantled by alteration that has the appearance of kelyphite. Many grains of dark red spinel have a cuspate form and some are intergrown with diopside. Sparse lenticles of garnet, 0.1 to 0.2 mm in width transect olivine and appear to fill fractures. The enstatite and spinel in this peridotite are inhomogeneous (see Table 1) and there is significant variability of Fe in the olivine. Flakes of graphite up to 2 mm in length are dispersed in a crude band that can be seen in hand specimen.

PHN5264 Premier. Strongly serpentinised coarse garnet-spinel lherzolite with olivine and abundant enstatite ranging up to 1 cm. Garnet is also abundant as irregularly shaped grains, some interstitial. Dark red cuspate spinel is included in garnet as well as interstitial to olivine and may represent a reaction relationship. Sparse diopside is associated with garnet. The enstatite and spinel are markedly inhomogeneous (Table 1) and the garnet has variable Ca and Cr. Two aggregates of graphite seen on the xenolith surface are associated with enstatite.

References

Bailey DK (1980) Volcanism, Earth degassing and replenished lithosphere mantle. Philos Trans R Soc London A297:309–322

Balhaus CG, Stumpfl EF (1985) Occurrence and petrological significance of graphite in the upper critical zone, W. Bushveld complex South Africa. Earth Planet Sci Lett 74:58–68

Bebout GE, Fogel MF (1990) Behaviour of nitrogen during metamorphism: case study of the Catalina schist subduction-zone metamorphic terrane. Annu Rep Dir Geophys Lab 1989–1990:19–26

Blundy JD, Brodholt JP, Wood BJ (1991) Carbon-fluid equilibria and the oxidation state of the upper mantle. Nature 349:321–324

Bobrievich AP, Smirnov GI, Sobolev VS (1959) An eclogite xenolith with diamonds (in Russian). Dokl Akad Nauk SSSR 126:637–640

Bottinga Y (1969) Carbon isotope fractionation between graphite, diamond and carbon dioxide. Earth Planet Sci Lett 5:301–307

Boyd FR (1989) Compositional distinction between oceanic and cratonic lithosphere. Earth Planet Sci Lett 96:15–26

Boyd FR, Finger LW (1975) Homogeneity of minerals in mantle rocks from Lesotho. Carnegie Inst Washington Yearb 74:519–525

Boyd FR, Finnerty AA (1980) Conditions of origin of natural diamonds of peridotite affinity. J Geophys Res 85:6911–6918

Boyd FR, Gurney JJ (1986) Diamonds and the African lithosphere. Science 232:472–477

Boyd FR, Nixon PH (1975) Origins of ultramafic nodules from some kimberlites of northern Lesotho and the Monastery Mine, South Africa. Phys Chem Earth 9:431–451

Boyd FR, Pearson DG, Nixon PH, Mertzman SA (1993) Low Ca garnet harzburgites from southern Africa: their relation to craton structure and diamond crystallisation. Contrib Mineral Petrol 113:352–366

Boyd SR, Pillinger CT, Milledge HJ, Mendelssohn MJ, Seal M (1992) C and N isotopic composition and the infrared absorption spectra of coated diamonds: evidence for regional uniformity of $CO_2 - H_2O$ rich fluids in the lithospheric mantle. Earth Planet Sci Lett 109:633–644

Brenan J, Watson EB (1988) Fluids in the lithosphere. 2. Experimental constraints on CO_2 transport in dunite and quartzite at elevated $P-T$ conditions with implications for mantle and crustal decarbonation processes. Earth Planet Sci Lett 91:141–158

Brey GP, Kohler T (1990) Geothermobarometry in four-phase lherzolites. II. New thermobarometers, and practical assessment of existing thermobarometers. J Petrol 31:1353–1378

Brey GP, Kogarko LN, Ryabchikov ID (1991) Carbon dioxide in kimberlitic melts. Neues Jahrb Mineral Monatsh 4:159–168

Bundy FP, Bovenkerk HP, Strong HM, Wentorf RH (1961) Diamond-graphite equilibrium line from growth and crystallisation of diamond. J Chem Phys 35:383–391

Canil D (1990) Experimental study bearing on the absence of carbonate in mantle-derived xenoliths. Geology 18:1011–1013

Canil D (1992) Orthopyroxene stability along the peridotite solidus and the origin of cratonic lithosphere beneath southern Africa. Earth Planet Sci Lett 111:83–95

Davies GR, Nixon PH, Pearson DG, Obata M (1993) Graphitised diamonds from the Ronda peridotite massif, S. Spain. Proc 5th Int Kimberlite Conf Brazil (in press)

Dawson JB, Smith JV (1975) Occurrence of diamond in a mica-garnet lherzolite xenolith from kimberlite. Nature 254:580–581

Deines P (1980) The carbon isotopic composition of diamonds: relationship to diamond shape, color, occurrence and vapour composition. Geochim Cosmochim Acta 44:943–961

Deines P (1991) Model simulations of carbon isotope variability in the mantle (abstract) Extended Abstr 5th Int Kimberlite Conf CPRM Spec Publ 2/91, Brasilia, pp 74–75

Deines P, Gold DP (1973) The isotopic composition of carbonatite and kimberlite carbonates and their bearing on the isotopic composition of deep seated carbon. Geochim Cosmochim Acta 49:89–95

Deines P, Gurney JJ, Harris JW (1984) Associated chemical and carbon isotopic composition variations in diamonds from Finsch and Premier kimberlite, South Africa. Geochim Cosmochim Act 48:325–342

Deines P, Harris JW, Gurney JJ (1987) Carbon isotopic composition, nitrogen content and inclusion composition of diamonds from the Roberts Victor kimberlite, South Africa. Geochim Cosmochim Acta 51:1227–1243

Deines P, Harris JW, Gurney JJ (1991) The carbon isotopic composition and nitrogen content of lithospheric and asthenospheric diamonds from the Jagersfontein and Koffiefontein kimberlite, South Africa. Geochim Cosmochim Acta 55:2615–2625

Duba AG, Shankland TG (1982) Free carbon and electrical conductivity in the Earth's mantle. Geophys Res Lett 9:1271–1274

Eggler DH, Baker DR (1982) Reduced volatiles in the system C–O–H: implications to mantle melting, fluid formation and diamond genesis. In: Akimoto S, Manghnani MH (eds) High pressure research in geophysics. Center for Academic Publications, Tokyo, pp 237–250

Everall NJ, Lumsdon J, Christopher DJ (1991) The effect of laser-induced heating opon the vibrational Raman spectra of graphite and carbon fibres. Carbon 29:133–137

Exley RA, Mattey DP, Clague DA, Pillinger CT (1986) Carbon isotope systematics of a mantle "hotspot": a comparison of Loihi Seamount and MORB glasses. Earth Planet Sci Lett 78:189–199

Field SW, Haggerty SE (1990) Graphitic xenoliths from the Jagersfontein kimberlite, South Africa: evidence for dominantly anhydrous melting and carbon deposition. Eos, Trans Am Geophys Union 71:658

Finnerty AA, Boyd FR (1984) Evaluation of thermobarometers for garnet peridotites. Geochim Cosmochim Acta 48:15–27

Finnerty AA, Boyd FR (1987) Thermobarometry for garnet peridotites: basis for the determination of thermal and compositional structure of the upper mantle. In: Nixon PH (ed) Mantle xenoliths. Wiley, London, pp 381–402

Galimov EM (1991) Isotope fractionation related to kimberlite magmatism and diamond formation. Geocheim Cosmochim Acta 55:diamond formation. Geochim Cosmochim Acta 55:1697–1708

Galimov EM, Solov'yeva LV, Belomestnykh AV (1989) Carbon isotope composition of metasomatised mantle rocks. Geokhimiya 4:508–514

Girod M (1967) Donnes petrographiques sur les pyroxenolites a grenat en enclaves dans les basaltes du Hoggar (Sahara Central). Bull Soc Fr Mineral Cristallogr 90:202–213

Griffin WL, Sobolev NV, Ryan CG, Pokhilenko NP, Win TT, Yefimova ES (1993) Trace elements in garnets and chromites: diamond formation in the Siberian lithosphere. Lithos 29:235–256

Gurney JJ (1991) The diamondiferous roots of our wondering continents. S Afr J Geol 93(3):424–437

Jaques AL, O'Neill HSt.C, Smith CB, Moon J, Chappell BW (1990) Diamondiferous peridotite xenoliths from the Argyle (AK1) lamproite pipe, Western Australia. Contrib Mineral Petrol 104:255–276

Javoy M, Pineau F, Delorme H (1986) Carbon and nitrogen isotopes in the mantle. Chem Geol 57:41–62

Kennedy CS, Kennedy GC (1976) The equilibrium boundary between diamond and graphite. J Geophys Res 81:2467–2470

Kennedy WQ (1964) The structural differentiation of Africa in the Pan African (±500 million years) tectonic episode. Rev Inst Afr Geol Eighth Annu Rep Sci Results. 1962–1963:48–49

Kornprobst J, Pineau F, Degiovanni R, Dautria JM (1987) Primary igneous graphite in ultramafic xenoliths: I. Petrology of the cumulate suite in alkai basalt near Tissemt (Eggéré, Algerian Sahara). J Petrology 28:293–311

Kropotova J, Fedorenko BV (1970) Carbon isotopic composition of diamond and graphite from eclogite. (in Russian) Geokhimiya 10:1279

Luth RW, Virgo D, Boyd FR, Wood BJ (1990) Ferric iron in mantle-derived garnets, implications for thermobarometry and for the oxidation state of the mantle. Contrib Mineral Petrol 104:56–72

Mathias M, Siebert JC, Rickwood PC (1970) Some aspects of the mineralogy and petrology of ultramafic xenoliths in kimberlite. Contrib Mineral Petrol 26:75–123

Mattey DP, Exley RA, Pillinger CT, Menzies MA, Porcelli DR, Galer S, O'Nions RK (1989) Relationships between C, He, Sr and Nd isotopes in mantle diopsides. In: Ross J et al. (eds) Kimberlites and related rocks, vol 2. Geol Soc Aust Spec Publ No. 14. Blackwell, Australia, pp 913–921

McKenzie DP (1989) Some remarks on the movement of small melt fractions in the mantle. Earth Planet Sci Lett 95:53–72

Morgan GB VI, Chou I-M, Pasteris JD, Olsen SN (1993) Re-equilibration of CO_2 fluid inclusions at controlled hydrogen fugacities: reaction mechanisms and open system behaviour. J Metamorphic Geol 11:155–164

Nadeau S, Pineau F, Javoy M, Francis D (1990) Carbon concentrations and isotopic ratios in fluid inclusion-bearing upper mantle xenoliths along the northwestern margin of north America. Chem Geol 81:271–297

Nixon PH, Boyd FR (1973a) Deep seated nodules. In: Nixon PH (ed) Lesotho Kimberlites. Cape and Transvaal, Cape Town, pp 106–109

Nixon PH, Boyd FR (1973b) Petrogenesis of the granular and sheared ultrabasic nodule suite in kimberlite. In: Nixon PH (ed) Lesotho Kimberlites. Cape and Transvaal, Cape Town, pp 48–56

Nixon PH, Boyd FR (1973c) The discrete nodule association in kimberlites in northern Lesotho. In: Nixon PH (ed) Lesotho kimberlites. Cape and Transvaal, Cape Town, pp 67–75

Nixon PH, van Calsteren PWC, Boyd FR, Hawkesworth CJ (1987) Harzburgites with garnets of diamond facies from southern African kimberlites. In: Nixon PH (ed) Mantle xenoliths. Wiley, London, pp 523–533

Pasteris JD (1981) Occurrence of graphite in serpentinized olivines in kimberlite. Geology 9:356–359

Pasteris JD (1987) Fluid inclusions in mantle xenoliths. In: Nixon PH (ed) Mantle xenoliths. Wiley, London, pp 691–707

Pasteris JD (1988) Secondary graphitization in mantle derived rocks. Geology 16:804–807

Pasteris JD, Wanamaker BJ (1988) Laser Raman microprobe analysis of experimentally re-equillibrated fluid inclusions in olivine: some implications for mantle fluids. Am Mineral 73:1074–1088

Pasteris JD, Wopenka B (1991) Raman spectra of "graphite" as indicators of degree of metamorphism. Can Mineral 29:1–9

Pearson DG, Davies GR, Nixon PH, Milledge HJ (1989) Graphitized diamonds from a peridotite massif in Morocco and implications for anomalous diamond occurrences. Nature 338:60–62

Pearson DG, Boyd FR, Nixon PH (1990) Graphite-bearing mantle xenoliths from the Kaapvaal craton: implications for graphite and diamond genesis. Carnegie Inst Washington Yearb, pp 11–19

Pearson DG, Davies GR, Nixon PH, Mattey DP (1991a) A carbon isotope study of diamond facies pyroxenites from the Beni Bousera peridotite massif, N. Morocco. In: Nicolas A, Dupuy C, Menzies MA (eds) Orogenic lherzolites and mantle processes. J Petrol Spec Issue, pp 175–189

Pearson DG, Shirey SB, Carlson RW, Boyd FR, Nixon PH, Pokhilenko NP, Brown L (1991b) Rhenium-osmium isotope systematics in southern African and Siberian peridotite xenoliths and the evolution of subcontinental lithospheric mantle (abstract). Extended Abstr 5th Int Kimberlite Conf, CPRM Spec Publ 2/91, Brasilia, pp 329–331

Pearson DG, Shirey SB, Carlson RW, Boyd FR, Pokhilenko NP, Nixon PH (1993) Re–Os isotope evidence for the formation of ancient lithospheric mantle linked to crust-building beneath southern Africa and Siberia. Terra Nova 5:40

Pineau F, Javoy M, Kornprobst J (1987) Primary igneous graphite in ultramafic xenoliths: II. Isotopic composition of the carbonaceous phases present in xenoliths and host lava at Tissemt, (Eggéré, Algerian Sahara). J Petrology 28:313–322

Pokhilenko NP, Sobolev NV, Yefimova ES (1982) Xenolith of deformed diamond-bearing kyanite eclogite from the Udachnaya pipe (in Russian). Dokl Akad Nauk SSSR 266:212–216

Pokhilenko NP, Pearson DG, Boyd FR, Sobolev NV (1991) Megacrystalline dunites: sources of Siberian diamonds. Carnegie Inst Washington Yearb: 11–18

Pollack HN (1986) Cratonization and thermal evolution of the mantle. Earth Planet Sci Lett 80:175–182

Richardson SH (1986) Latter-day origin of diamonds of eclogite paragenesis. Nature 322:623–626
Richardson SH, Gurney JJ, Erlank AJ, Harris JW (1984) Origin of diamonds in old enriched mantle. Nature 310:198–202
Robinson DN (1979) Diamond and graphite in eclogite xenoliths from kimberlite. In: Boyd FR, Meyer HOA (eds) The mantle sample. AGU, Washington, pp 50–58
Robinson DN, Gurney JJ, Shee SR (1984) Diamond eclogite and graphite eclogite xenoliths from Orapa, Botswana. In: Kornprobst J (ed) Kimberlites. II. The mantle and crust-mantle relationships. Elsevier, Amsterdam, pp 11–24
Rodionov AS, Sobolev NV (1985) A new find of a xenolith of graphite-bearing harzburgite (in Russian). Geol Geofiz 26:32–37
Rudnick RL, Eldridge CS, Bulanova GP (1992) Diamond growth history from in situ measurement of Pb and S isotopic compositions of sulphide inclusions. Geology 26:13–16
Rumble D, Hoering TC (1986) Carbon isotope geochemistry of graphite vein deposits from New Hampshire, USA. Geochim Cosmochim Acta 50:1239–1247
Schulze DJ (1986) Calcium anomalies in the mantle and a subducted metaserpentinite origin for diamonds. Nature 319:483–485
Schulze DJ, Valley JW (1991) Carbon isotope composition of mantle graphite: anomalously light carbon subducted into the shallow subcontinental lithosphere (abstract) Geol Assoc Can/Mineral Assoc Can
Shee SR, Gurney JJ, Robinson DN (1982) Two diamond-bearing peridotite xenoliths from the Finsch kimberlite, South Africa. Contrib Mineral Petrol 81:79–87
Schulze DJ, Valley JW, Viljoen KS, Spicuzza M (1991) Carbon isotope composition of graphite in mantle eclogites (abstract). Extended Abstr 5th Int Kimberlite Conf (CPRM Spec Publ 2/91, Brasilia), pp 353–355
Smith CB, Gurney JJ, Harris JW, Otter ML, Kirkley MB, Jagoutz E (1991) Neodymium and strontium isotope systematics of eclogite and websterite paragenesis inclusions from single diamonds, Finsch and Kimberley Pool, RSA. Geochim Cosmochim Acta 55:2579–2590
Sobolev NV (1974) Deep-seated inclusions in kimberlites and the problem of the composition of the upper mantle (in Russian). Nauka, Novosibirsk
Sobolev NV, Galimov EM, Ivanovskaya IN, Yefimova ES (1979) The carbon isotope compositions of diamonds containing crystalline inclusions. Dokl Akad Nauk SSSR 249:1217–1220
Sobolev NV, Pokhilenko NV, Yefimova ES (1984) Diamond-bearing peridotite xenoliths in kimberlite and the problem of the origin of diamonds (in English). Geol Geofiz 25:63–80; English translation, Sov Geol Geophys 25:62–76
Sobolev VS, Sobolev NV (1980) New proof of a very deep subsidence of eclogitised crustal rocks (in Russian). Dokl Akad Nausk SSSR 250:683–685
Spera FJ (1984) Carbon diaoxide in petrogenesis III: role of volatiles in the ascent of alkaline magma with special reference to xenolith-bearing mafic lavas. Contrib Mineral Petrol 88:217–232
Taylor BE (1986) Magmatic volatiles: Isotopic variation of C, H and S. In: Valley JW, Taylor HP, O'Neil JR (eds) Stable isotopes in high temperature geological processes. Mineral Soc Am Spec Publ 16, pp 185–219
Taylor WR, Green DH (1989) The role of reduced C–O–H fluids in mantle partial melting. In: Ross J et al. (eds) Kimberlites and related rocks, vol 1. Geol Soc Aust Spec publ No. 14. Blackwell, Australia, pp 592–602
Viljoen KS, Swash PM, Otter ML, Schulze DJ, Lawless PJ (1992) Diamondiferous garnet harzburgites from the Finsch kimberlite, North Cape, South Africa. Contrib Mineral Petrol 110:133–138
Viljoen KS, Robinson DN, Swash PM, Griffin WL, Otter ML, Ryan CG, Win TT (1993) Diamond- and graphite-bearing peridotite xenoliths from the Roberts Victor kimberlite, South Africa. Proc 5th Int Kimberlite Conf Brazil (in press)
Wagner PA (1916) Graphite-bearing xenoliths from the the Jagersfontein mine. Geol Soc S Afr Trans 19:54–56
Walker RJ, Carlson RW, Shirey SB, Boyd FR (1989) Os, Sr, Nd and Pb isotope systematics of southern African peridotite xenoliths: implications for the chemical evolution of subcontinental mantle. Geochim Cosmochim Acta 53:1583–1595
Watson EB, Brenan JM, Baker DR (1990) Distribution of fluid in the continental lithosphere, In: MA Menzies (ed) Continental mantle. Clarendon Press, Oxford, pp 111–125
Woermann E, Rosenhauer M (1985) Fluid phases and the redox state of the Earth's mantle. Extrapolations based on experimental, phase theoretical and petrological data. Fortschr Mineral 63:262–349
Wood BJ (1991) Oxygen barometry of spinel peridotites. In: Lindsley DH (ed) Oxides petrological and magnetic significance. Mineral Soc Am Spec Publ 25, pp 417–431
Wopenka B, Pasteris JD (1993) Structural characterisation of kerogen to granulite facies graphite: applicability of Raman microprobe spectroscopy. Am Mineral (in press)

Editorial responsibility: W. Schreyer